Tungsten (2020) 2:337–361
https://doi.org/10.1007/s42864-020-00068-0

Tungsten
www.springer.com/42864

REVIEW PAPER

Self-supported transition metal oxide electrodes for electrochemical energy storage

Xiao-Ling Teng[1] · Xi-Tong Sun[1] · Lu Guan[1] · Han Hu[1] · Ming-Bo Wu[1]

Received: 16 September 2020 / Revised: 20 October 2020 / Accepted: 20 October 2020 / Published online: 17 December 2020

Abstract
Electrode materials are of decisive importance in determining the performance of electrochemical energy storage (EES) devices. Typically, the electrode materials are physically mixed with polymer binders and conductive additives, which are then loaded on the current collectors to function in real devices. Such a configuration inevitably reduces the content of active species and introduces quite some undesired interfaces that bring down the energy densities and power capabilities. One viable solution to address this issue is to construct self-supported electrodes where the active species, for example transition metal oxides (TMOs), are directly integrated with conductive substrates without polymer binders and conductive additives. In this review, the recent progress of self-supported TMO-based electrodes for EES devices including lithium-ion batteries (LIBs), sodium-ion batteries (SIBs), aluminum-ion batteries (AIBs), metal-air batteries, and supercapacitors (SCs), is discussed in great detail. The focused attention is firstly concentrated on their structural design and controllable synthesis. Then, the mechanism understanding of the enhanced electrochemical performance is presented. Finally, the challenges and prospects of self-supported TMO-based electrodes are summarized to end this review.

Keywords Self-supported electrodes · Transition metal oxides · Metal-ion batteries · Metal-air batteries · Supercapacitors

1 Introduction

The immoderate consumption of fossil fuels (coal, oil, natural gas, etc.) for years has resulted in the imminent shortage of these non-renewable resources, environmental pollutions, and greenhouse effects. In this context, renewable energy is widely exploited to revolutionize our current energy structure for a sustainable world [1–7]. Nevertheless, these renewable sources are highly fluctuant and intermittent making their reliable utilization challenging. To address these intractable issues, the rational combination of them with electrochemical energy storage (EES) devices is highly recognized as a viable solution. Typically, the EES devices can be divided into high-energy density devices, namely batteries (such as lithium-ion batteries (LIBs), sodium-ion batteries (SIBs), aluminum-ion batteries (AIBs), metal-air batteries, and so on), and power capable systems, for example supercapacitors (SCs) based on the principle of electrochemical processes [8–15]. The practical performance of these devices is highly dependent on the properties of the electrode materials. To function in the final devices, the electrode materials have to be physically mixed with the conductive additives and polymer binders which are then coated on the metal current collectors as illustrated in Fig. 1a. Such a slurry-casting electrode usually suffers from several drawbacks. The large interface resistance resulting from a large number of grain boundaries brings about undesirable interfaces declining the charge transport. Then, the auxiliary components including polymer binders and conductive additives have some adverse effects on the specific capacity. Specifically, these additives occupy a high content in the electrodes and reduce the specific capacities [16–18]. Recently, the rational design and construction of self-supported electrodes have aroused widespread attention for their capability to effectively solve these drawbacks. Self-supported electrodes refer to electrodes where the active species are directly integrated with the conductive substrates through the in-situ growth of active species on

✉ Han Hu
hhu@upc.edu.cn

✉ Ming-Bo Wu
wumb@upc.edu.cn

[1] State Key Lab of Heavy Oil Processing, Institute of New Energy, College of Chemical Engineering, China University of Petroleum (East China), Qingdao 266580, China

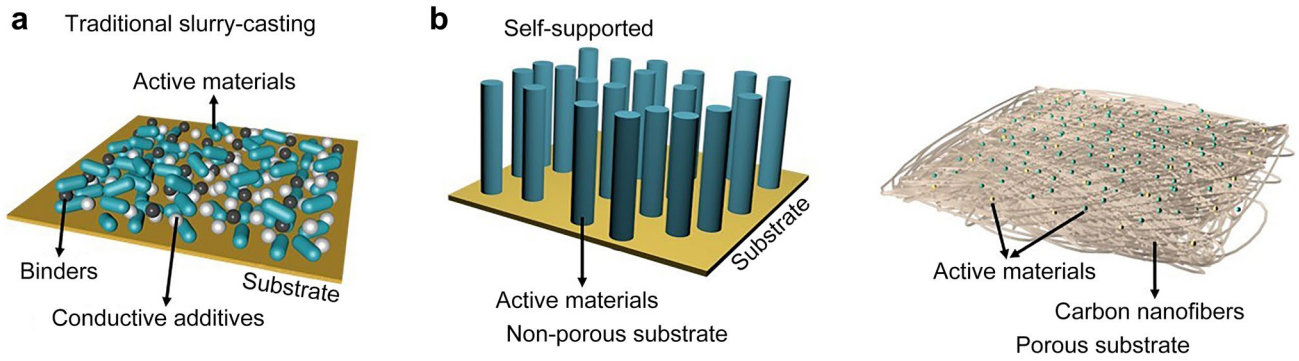

Fig. 1 Schematic illustration of the structural and electrochemical features of: **a** traditional slurry-casting electrode that the active materials coated on substrate along with the polymer binders and conductive additives, **b** self-supported electrodes with in situ grown active materials on the current collectors and co-assembled active materials and conductive networks

the current collectors or by the assembly of active materials with conductive materials into free-standing architectures, as illustrated in Fig. 1b [19–26]. In contrast to the traditional slurry-casting electrodes, their self-supported counterparts eliminate the use of binders and conductive additives, which not only simplify the electrode processing but also boost the energy density of the EES devices. Besides, the active species can strongly adhere to the substrate that essentially reduces the contact resistance and allow rapid charge transfer [27, 28]. TMOs have been widely considered as versatile electrode materials for both batteries and SCs [29–33]. Due to the rich selection of transition metals, a wide range of TMOs have been demonstrated as powerful electrodes for many energy storage applications, which makes the self-supported TMO electrodes for EES devices a burgeoning research field.

In this review, the recent progress of this emerging topic has been elaborately summarized. Firstly, the state-of-the-art methods to fabricate these electrodes are discussed. Then, some typical examples of self-supported TMO electrodes for use in LIBs, SIBs, AIBs, metal-air batteries, and SCs are discussed to demonstrate their potential in the future EES devices as shown in Fig. 2. Finally, the existing challenges and prospects in this research field are discussed to shed some light on the further development of the prospective field.

2 Design and synthesis of self-supported TMOs electrodes

The self-supported electrodes can be prepared either by in-situ integrating active species on the monolithic substrates or through the assembly of the electrode materials and conductive components into free-standing structures. The typical technologies employed in the fabrication processed include hydro/solvothermal synthesis, electrodeposition, vacuum filtration, pulsed laser deposition (PLD), chemical vapor deposition (CVD), and atomic layer deposition (ALD), to name a few. The progress of the aforementioned two-types of self-supported electrodes is discussed below.

2.1 In-situ growth strategies for preparing self-supported electrodes

2.1.1 Self-supported electrodes based on metal foil substrates

To construct self-supported electrodes through the in-situ growth technologies, the first step is to select a highly conductive substrate, among which the metal foils represent the most widely employed one. Metal-based substrates possess outstanding structural stability and conductivity, and the directly grown active species generally show stronger adhesion to such substrates as well as prohibit the use of conductive additives and polymer binders. Typical examples include Cu foils, Ti foils, stainless steel meshes, and so on, as illustrated in Fig. 2.

The Cu foil is the most commonly used anode current collector for LIBs in the traditional slurry-casting method which makes the Cu foil the choice of substrates for self-supported anodes of LIBs [34, 35, 36]. Cao et al. [37] have fabricated hierarchical CoO nanowire clusters (NWCs) on a pre-treated Cu foil via hydrothermal and annealing treatments which is directly applied as the anode of LIBs (Fig. 3a). The nanowires (NWs) compose of self-assembled ultra-small nanoparticles (NPs) (≈10 nm) contributing to a hierarchical structure. This strategy has then been extended to fabricate self-supported electrodes made of other active species, such as CuO nanorod arrays (NRAs) [19, 38], TiO_2/reduced graphene oxide (rGO) nanocomposite [39], $Co_xMn_yNi_zO$ nanosheets (NSs) or NWs, [40]. Teng et al. [41] used the PLD to construct low crystalized films made of Fe_2O_3 NPs on the Cu foil as the anode of LIBs. Then,

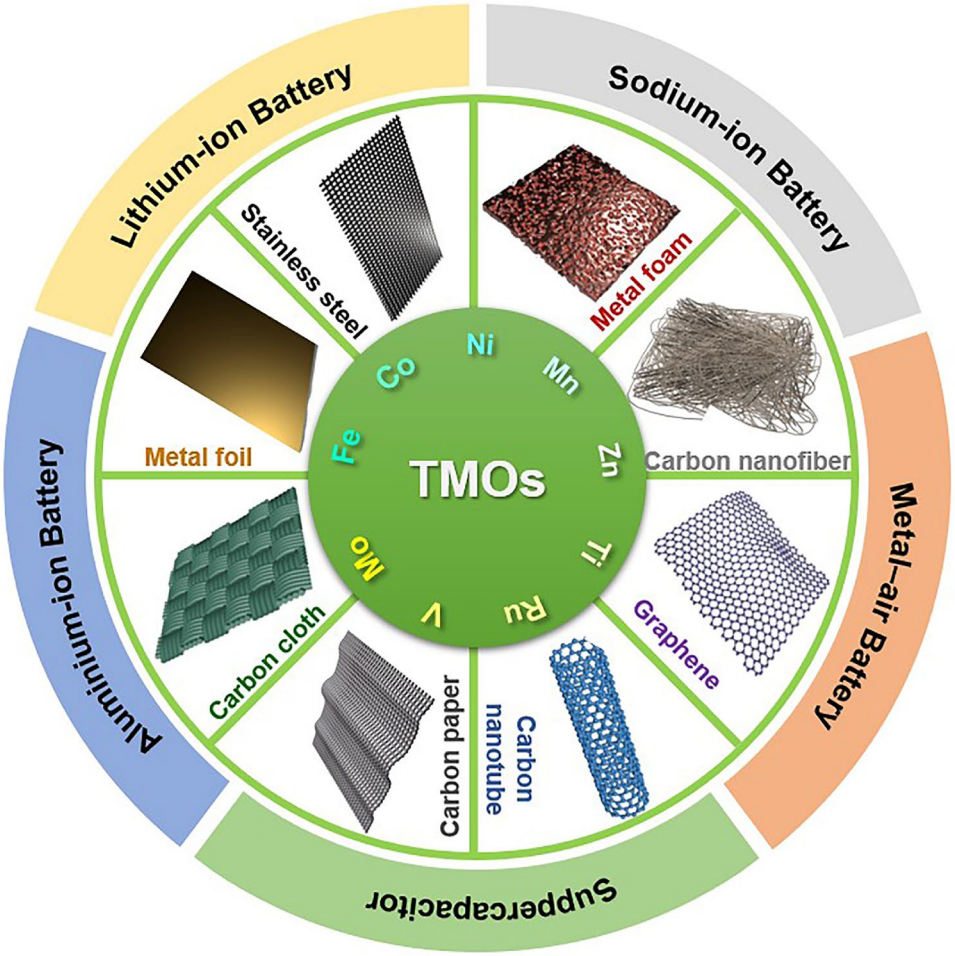

Fig. 2 Design and synthesis strategies of self-supported TMOs and their applications in EES

a hybrid film comprised of SnO_2 and TiO_2 NPs were prepared by alternative deposition of active species using PLD [42]. The average thickness of the SnO_2 and TiO_2 is 60 and 10 nm, respectively, and the alternative deposition of them three times contributed to a hybrids film with a thickness of 210 nm. The PLD process shows high applicability and a wide range of metal oxides, such as NiO, CoO, and so on, have been successfully deposited on the Cu foil for robust lithium storage [43, 44]. Because of the excellent conductivity, the Cu foil could also be integrated with the electrochemical deposition process where the amorphous TiO_2 nanotube arrays were firmly attached on the Cu foil [45].

In addition to exclusively serving as the current collectors, the metal substrate can also be directly converted into active species. For example, the surface of Cu foil was converted into CuO which was then hybridized with SnO_2 for synergistic lithium storage [46]. Yuan et al. [38] realized a facile and scalable in-situ Cu foil engraving modus to prepare a self-supported electrode where CuO NRAs are integrated with the porous Cu framework. Chen et al. [47] used a facile and effective gas-etch method to directly grow $CuO/Cu(OH)_2$ composite on the Cu foil at the ambient temperature. Li et al. [48] successfully prepared porous leaf-like CuO nanoplate arrays electrode on the Cu foil by wet chemical oxidation method. All of these self-supported structures possess ample open space and high specific surface area facilitating the electrolyte migration for enhanced electrochemical performance. In addition to Cu foil, Co foils have also been employed for this purpose. Liang et al. [49] reported an in-situ grown nanocotton-like CoO on the surface of the Co foil via a laser ablation strategy (Fig. 3b). The as-obtained self-supported electrodes not only have a large specific area but also a firm collection between the active materials and current collectors which provides a rapid electronic conduction path. In addition, there are many other researches related to Co-based materials, such as hierarchical $Co_3O_4/rGO/Co_3O_4$ pseudocomposite [50].

Both Cu and Co foils are relatively active which can be corroded during the electrochemical processes. To address this issue, the highly stable Ti foil has been suggested to directly loading active species, among which TiO_2 of different morphologies, as film [51], nanowires [52], and nanotubes [53] have been directly loaded. For the enhanced connection with the active materials, Ti NWs array has

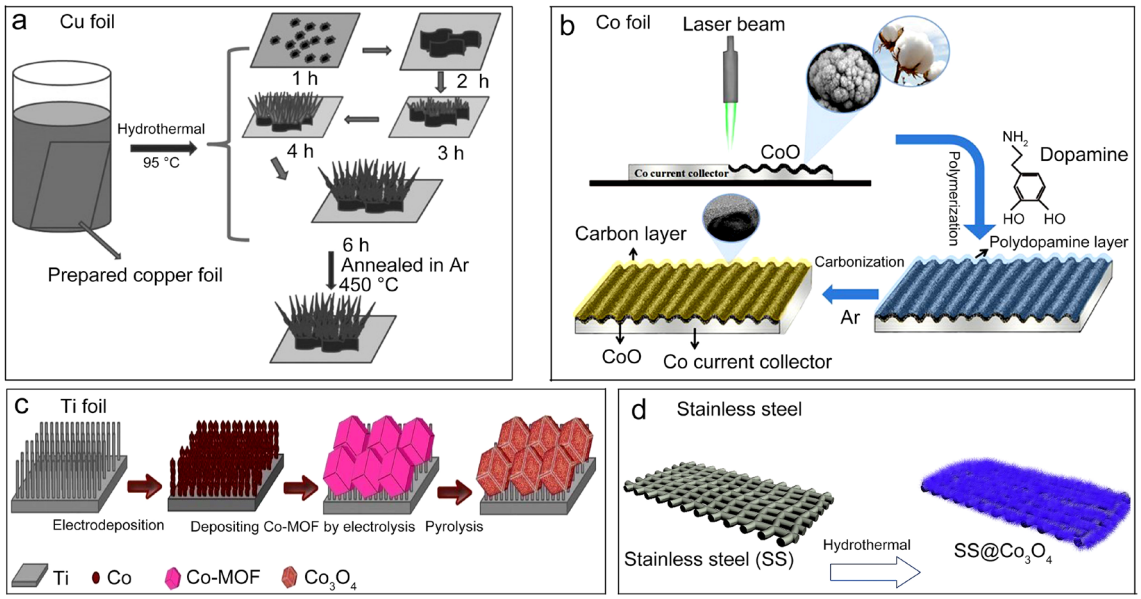

Fig. 3 Schematic illustration of the formation of **a** hierarchical CoO NWCs; Reproduced with permission from Ref. [37]. Copyright 2015, Wiley. **b** CoO@C-Co on Co foil. Reproduced with permission from Ref. [49]. Copyright 2019, Wiley. **c** Co-MOF derived Co_3O_4 on Ti NWAs; Reproduced with permission from Ref. [54]. Copyright 2018, Elsevier. **d** Co_3O_4 on SS. Reproduced with permission from Ref. [57]. Copyright 2020, Elsevier

been anchored on the surface of Ti foils which can penetrate deeply into the network of active species. As shown in Fig. 3c, Zhao et al. [54] introduced Co-based MOFs (Metal–Organic Frameworks) among the Ti NWs, which were then converted into nanostructured Co_3O_4. The metallic Ti NWs are interconnected with the Co_3O_4 scaffold that enhances the electron transport. Stainless steel (SS)-mesh is another widely used substrate that is strongly oxidation-resistant for self-supported electrodes [55, 56]. Wu et al. [57] fabricated cobalt carbonated hydroxide NWs grown on smooth SS through a hydrothermal method ($SS@Co_3O_4$) and the schematic illustration is shown in Fig. 3d. The substrate is in strong contact with the active materials, which contributes to a low internal resistance.

2.1.2 Self-supported electrodes based on porous metal substrates

The aforementioned metal foils possessing a relatively small specific surface area and are not conducive to load a large number of active materials. In recent years, lots of efforts have been made for developing highly porous metal structures to increase the loading amount of active species [58–60]. In this context, three-dimensional (3D) metal textures (e.g., porous Ni, Cu, and Au) have been employed for spacious loading of active species. The most widely employed one is the nickel foam (NF) because of its low cost and facile availability [61–73]. The successful examples include CoP_3/carbon polyhedron/CoO/NF nanoarrays [74], flower-type $NiCo_2O_4$/3D graphene-coated NF (3D-GNF) composite [75], porous NiO nanofibers [76], NiO nanorods [77], and so on. Han et al. [78] fabricated the Co_3O_4 nanohorns on NF (Co_3O_4/Ni) by a hydrothermal method (Fig. 4a) where the large-scale, dense, and uniform Co_3O_4 nanohorns are vertically grown on the skeleton of the NF to form a highly porous structure. Then, the nanoplate array of MnO_2 was collected on the nanohorns for a hybrid structure. Yuan et al. [79] reported a self-supported composite anode composed of CuO NSs and multi-wall CNTs (MWCNTs) for LIBs (Fig. 4b). The copper was firstly plated on the skeleton of NF. Then, a layer of MWCNTs was coated on the framework through an electrophoretic deposition (EPD) process. After that, the plated Cu was in-situ converted into CuO nanoplates that are interconnected with the MWCNTs for improved conductivity. Despite the great success of employing NFs to load active species for self-supported electrodes, the as-prepared electrodes still contain a high-portion of the void because of the ultra-large pores within the NF that limit the boosting of energy density. As a result, the size of the porous metal current collectors should be essentially reduced to avoid the waste of space. Liu et al. [80] have reported a versatile dealloying process ($Cu_{50}Al_{50}$ (wt%) alloy was chosen as the precursor) to generate 3D nanoporous Cu (NPCu) foams which were then loaded with Cu_2O layers for reversible lithium storage (Fig. 4c). The NPCu revealed a bi-continuous nanoporous structure composed of quasi-periodic copper ligaments and nanopore channels (Fig. 4d) and the size of these pores is much smaller than that of NF.

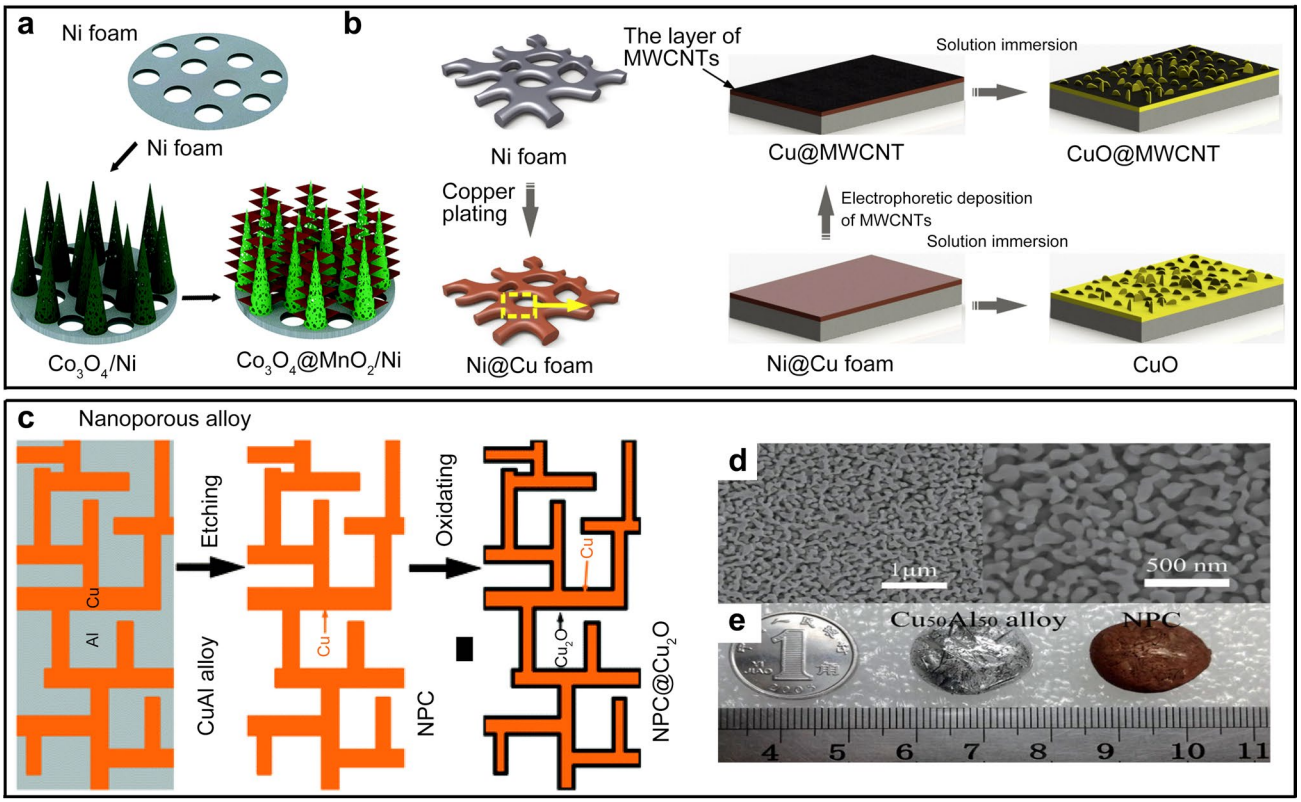

Fig. 4 Preparation procedure of **a** the Co_3O_4@MnO_2/Ni nanocomposite [78]. Reproduced with permission from Ref. [78]. Copyright 2016, The Royal Society of Chemistry (RSC). **b** binder-free CuO NSs@MWCNTs [79]. Reproduced with permission from Ref. [79]. Copyright 2018, Elsevier. **c** 3D NPCu@Cu_2O anodes, **d** SEM micrographs of NPCu foams produced by dealloying $Cu_{50}Al_{50}$, and **e** digital picture of $Cu_{50}Al_{50}$ alloy and NPCu foam. Reproduced with permission from Ref. [80]. Copyright 2013, RSC

In this regard, the invalid void is significantly reduced. A digital picture of a $Cu_{50}Al_{50}$ alloy and NPCu foam is shown in Fig. 4e. Such self-supported electrodes show excellent performances because of their good conductivity, mechanical properties, and interconnected porous channels for rapid ions diffusion.

2.1.3 Self-supported electrodes based on porous-carbon substrates

Despite the versatility of porous metal frameworks for constructing self-supported electrodes, the relatively high density of metal elements still limits the content of active species. As a result, porous, flexible, conductive, and stable frameworks made of lighter elements will be appealing. Monolithic carbon-based substrates perfectly combine the above-mentioned characters together and have been widely used to construct self-supported electrodes [81–86]. Quite some of these substrates, such as carbon cloth (CC) and carbon fiber paper (CFP), have already been commercially available, resulting in a large number of self-supported electrode based on them. For example, Sun et al. [23] presented the synthesis of 3D array anode of hematite grown on the flexible CC substrate (denoted as N-Fe_2O_{3-x}/CC). The fabrication involves a two-step sequential process as shown in Fig. 5a. As shown from the scanning electron microscopy (SEM) observation, (Fig. 5b-d) the nanorods of N-Fe_2O_{3-x} /CC showed evident shrinkage and clear split, and such a morphological change results in a larger specific surface area favoring the charge-transfer reaction and ion transport during cycling. Wang et al. [87] firstly combined the facile hydrothermal method and PVD (pulse vapor deposition) to prepare a self-supported α-Fe_2O_3@Si@C/CC electrode. The strategy is schematically illustrated in Fig. 5e. The as-prepared structure was directly used as a flexible anode for LIBs, which can largely improve the mass-loading of active material and exhibit a simultaneous improvement of specific capacity and cycling performance.

CFPs are another kind of carbon-based substrate to support active materials. Their texture is woven by CNFs with high flexibility and conductivity, making them unique supporting backbones for the controlled growth of active materials for EES. Shen et al. [88] have successfully fabricated $NiCo_2O_4$ NWAs covered on carbon textiles by a surfactant-assisted hydrothermal method combined with a post-annealing treatment (Fig. 5f). The NiCo-precursor can be easily

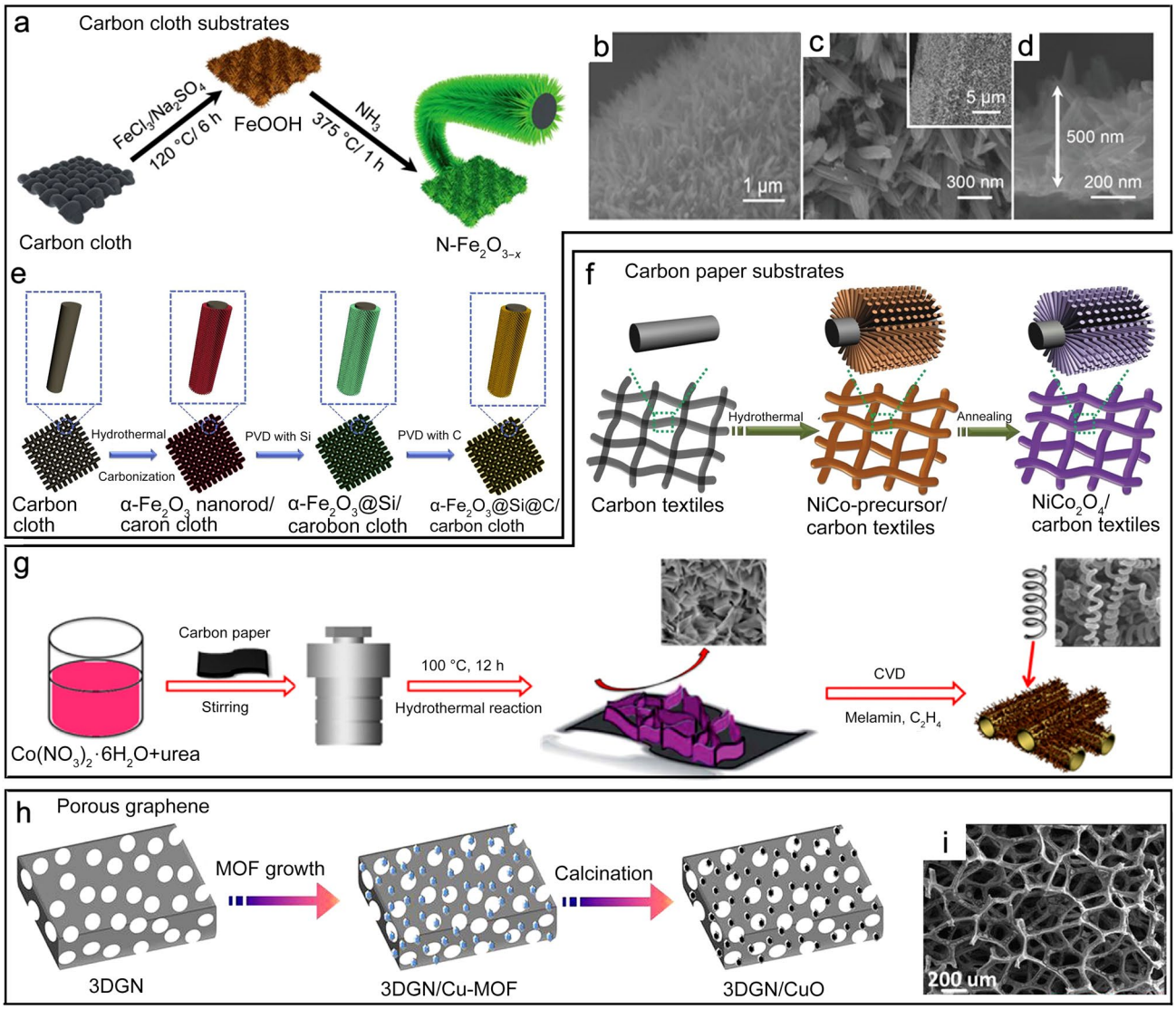

Fig. 5 **a** Synthesis and morphological characterization and **b–d** SEM images of N-Fe_2O_{3-x}/CC. Inset is zoomed-out image. Reproduced with permission from Ref. [23]. Copyright 2020, Wiley. Schematic illustration of the synthesis procedure for **e** a-Fe_2O_3@Si@C/CC electrode. Reproduced with permission from Ref. [87]. Copyright 2018, Elsevier. **f** $NiCo_2O_4$ NWAs/carbon textiles composite. Reproduced with permission from Ref. [88]. Copyright 2014, Wiley. **g** Co@CoO_x/HNCNTs. Reproduced with permission from Ref. [90]. Copyright 2020, American Chemical Society (ACS). **h** Illustration and **i** SEM images of the 3DGN/CuO electrode. Reproduced with permission from Ref. [91]. Copyright 2017, Elsevier

grown on the flexible carbon textiles under the hydrothermal condition and form a large-scale conformal coating. More importantly, $NiCo_2O_4$ nanowire have independent electrical contact with the underlying carbon fibers, and can be easily extended to grown other TMOs nanostructure on carbon-based substrates. Chen et al. [89] deposited nanostructured α-MnO_2 directly on CFP by a simple electrochemical process. Comparing with the conventional electrodes, the self-supported α-MnO_2@CFP electrode exhibits a higher capacitance and better rate capability. In another attempt as shown in Fig. 5g, Liu et al. [90] prepared high-purity Co@CoO_x/helical CNTs (HNCNTs) on a CFP by a hydrothermal treatment and subsequent CVD.

Graphene, an atomic-thick two-dimensional NSs made of honeycomb-packed carbon atoms, is widely considered as an ideal choice of materials for EES because of its exceptional electronic conductivity, excellent mechanical flexibility, large specific surface area, and light-weight. Ji et al. [91] obtained 3D graphene network and MOF-derived octahedral CuO (3DGN/CuO) composites as a self-supported anode of LIBs. As shown in Fig. 5h, the CVD-derived graphene replicated the 3D network and porous structure of the NF after removal of the Ni template

and the obtained 3DGN/CuO bulk material (Fig. 5i) can still keep the completeness after annealing 3DGN/Cu-MOF in air.

2.2 Assembling of active materials with conductive materials for the preparation of self-supported electrodes

To improve the electronic conductivity and mechanical strain of self-supported materials, nanostructured carbon materials (graphene, carbon nanofibers (CNFs), CNTs, etc.) were employed to assemble with TMOs, where carbon materials acted as conductive networks to increase the electrical conductivities and as volume buffers to alleviate internal stress during the cycling process.

Liu et al. [92] fabricated a flexible CuO NSs/rGO hybrid lamellar paper by the combined use of vacuum filtration and a subsequent hydrothermal reduction process. In the synthesis of the CuO NSs/rGO paper (Fig. 6a), the positively charged CuO NSs quickly interacted with the negatively charged GO sheets during the vigorous stirring of the mixed suspensions of GO and as-prepared CuO NSs. Then, a vacuum filtration process was applied to produce a free-standing paper where the CuO NSs were homogeneously embedded within the GO layers, giving rise to a sandwiched structure with good flexibility. After the hydrothermal treatment, the GO was reduced and the interaction between the two components was enhanced.

The combination of CNF mats with TMOs is also considered to be a good candidate of self-supported electrodes. As shown in Fig. 6b, Zhang et al. [93] combined the

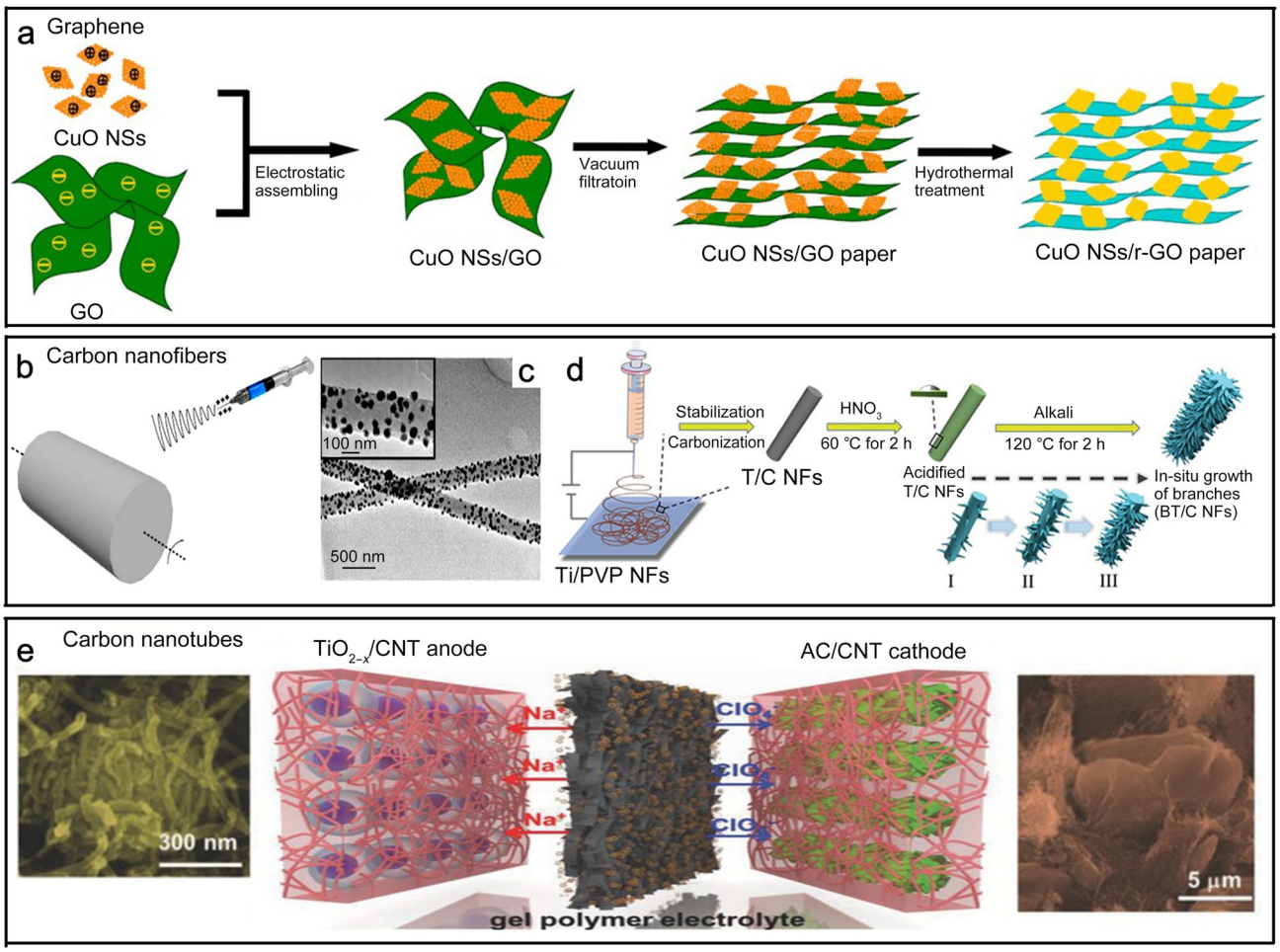

Fig. 6 **a** Schematic progress of CuO NSs/rGO Paper. Reproduced with permission from Ref. [92]. Copyright 2013, ACS. **b** Schematic illustrations of the electrospinning process and digital photograph of hybrid films during different heat treatment processes; **c** TEM image of $NiFe_2O_4$-CNFs, and inset is HRTEM image of $NiFe_2O_4$-CNFs. Reproduced with permission from Ref. [93]. Copyright 2018, Elsevier. **d** Illustration of the BT/C NFs. Reproduced with permission from Ref. [94]. Copyright 2019, Wiley. **e** Illustration of the flexible quasi-solid-state TiO_{2-x}/CNTs//AC/CNTs device (and the corresponding SEM images of flexible TiO_{2-x}/CNTs anode). Reproduced with permission from Ref. [97]. Copyright 2018, Wiley

free-standing 3D CNFs films with highly active $NiFe_2O_4$ catalysts ($NiFe_2O_4$-CNFs) as the air cathode for Li-O_2 batteries. The structural details are reflected from the transmission electron microscope (TEM) image (Fig. 6c) where numerous $NiFe_2O_4$ NPs are firmly embedded into nanofibers reflected from the high-resolution TEM (HRTEM) image in Fig. 6c. In addition, the unique 3D networks facilitate the immersion of electrolytes for promoted diffusion of O_2 and Li^+, and accommodate adequate discharge products. Wang and his colleagues [94] also used the electrospinning and alkali hydrothermal treatment method to prepare self-supported branched TiO_2/CNFs (BT/CNFs). The schematic illustration of the synthesis process of the BT/CNFs is shown in Fig. 6d, the as-obtained fibers were fabricated by electrospinning and then carbonized into flexible BT/CNFs. Apart from the aforementioned examples, many other TMOs composite nanofibers are prepared by electrospinning technology [95, 96]. These TMOs composite electrodes usually offered superior cycle and rate performance with a high area density.

CNTs, a tubular structure made up of rolled graphene NSs, possess excellent flexibility and conductivity. The CNTs can be fabricated into free-standing porous networks through a facile solution-processing process. The embeddedness of TMOs into the self-supported CNTs networks can effectively enhance the electrode conductivity and reduce the electrode weight to improve electrochemical properties. A myriad of free-standing electrodes based on the CNTs network, such as WS_2/CNTs-rGO [36], $Ni_{1.5}Co_{0.5}P_x$/CNTs [37] and P/CNTs@rGO [38], have been fabricated. Figure 6e illustrated an EES device with CNTs networks-based anode and cathode [97]. The anode is the oxygen-deficient TiO_{2-x}/CNTs battery-type anodes while the cathode consists of activated carbon (AC) particles embedded CNTs networks. Both of these two electrodes were prepared by a flow-direct assembly of the active species and CNTs. Wang et al. [98] showed that Fe_2O_3/single-walled carbon nanotube (SWNT) composites have the potential application as nanostructured electrodes for various energy devices such as SCs and LIBs. The SWNT films were continuously synthesized by using a CVD technique where Fe_2O_3 particles were distributed uniformly to occupy the void among the SWNT bundles. Besides, the remaining SWNTs maintain their original continuous interconnected network which is critical for forming stable self-supported electrode with good mechanical and electrical properties. In addition, this fabrication method is tunable and low-cost, and can be expanded to prepare other transition metal compounds/carbon composites with potential applications in flexible membrane electrodes.

3 Self-supported TMO-based electrode materials for EES

3.1 LIBs

TMOs have been considered as promising electrode materials for LIBs because of their multiple chemical valences and morphological characteristics. TMO-based anodes mainly include "NaCl structure" such as MnO, NiO, FeO, CoO, and CuO_2, high-valent oxides including MnO_2, Fe_2O_3, Fe_3O_4, Co_3O_4, and CuO, and bimetallic oxides such as ZnCoO, NiFeO, ZnFeO, etc. In contrast to the commercially available graphite anode, the TMO-based electrodes have high operating voltages securing improved safety. In general, TMO-based electrodes store lithium ions either using the conversion reaction or the intercalation process which are described below (Eqs. (1)-(2)):

$$\text{Conversion reaction: } M_xO_y + 2y\,Li^+ + 2ye^- \leftrightarrow y\,Li_2O + x\,M \quad (1)$$

$$\text{Intercalation reaction: } M_xO_y + nLi^+ + ne^- \leftrightarrow Li_nM_xO_y \quad (2)$$

The conversion type anodes consist of iron oxides [99, 100] cobalt oxides, [101, 102] nickel oxides, [103, 104] manganese oxides, [105–107] and so on, which generally possess high theoretical specific capacities. Du et al. [74] developed a facile strategy to design self-supporting CoP_3/carbon polyhedron (CP)/CoO on the NF for LIBs to reach a high specific capacity, the preparation process is shown in Fig. 7a The internal CoO NWs with a unique microstructure act as bridges to link NF and CoP_3/CP (Fig. 7b, c) which not only reinforces the adhesion between active material and NF but also enhances the capacity of whole electrode. As a result, the CoP_3/CP/CoO/NF anode exhibits an outstanding specific capacity of 1715 $mAh{\cdot}g^{-1}$ at 0.5 $A{\cdot}g^{-1}$ which can remain at 1150 $mAh{\cdot}g^{-1}$ after 80 cycles (Fig. 7d), demonstrating the good durability. In another attempt, Shao et al. [82] prepared the Fe_2O_3/CC electrode through conversion of CC supported Prussian blue (PB/CC). Because of the high mechanical strength and flexibility of the CC, the composite electrode maintained a self-standing structure without any collapse and destruction after the high-temperature treatment. Compared with pure CC and Fe_2O_3, the composite exhibited a higher mass and areal specific capacity, better electrochemical performances as the anode for LIBs. The mass specific capacity of Fe_2O_3/CC was about 395 $mAh{\cdot}g^{-1}$ (an area capacity of 5.1 $mAh{\cdot}g^{-1}$) at 100 $mA{\cdot}g^{-1}$ with almost no decay after 135 discharge/charge cycles. Specifically, the TMOs contribute to a high lithium storage capacity while the close contact between Fe_2O_3 and CC improves the cycle stability of electrode. The specific capacity of Fe_2O_3/CC is 121 $mAh{\cdot}g^{-1}$ even at a high current density (500 $mA{\cdot}g^{-1}$).

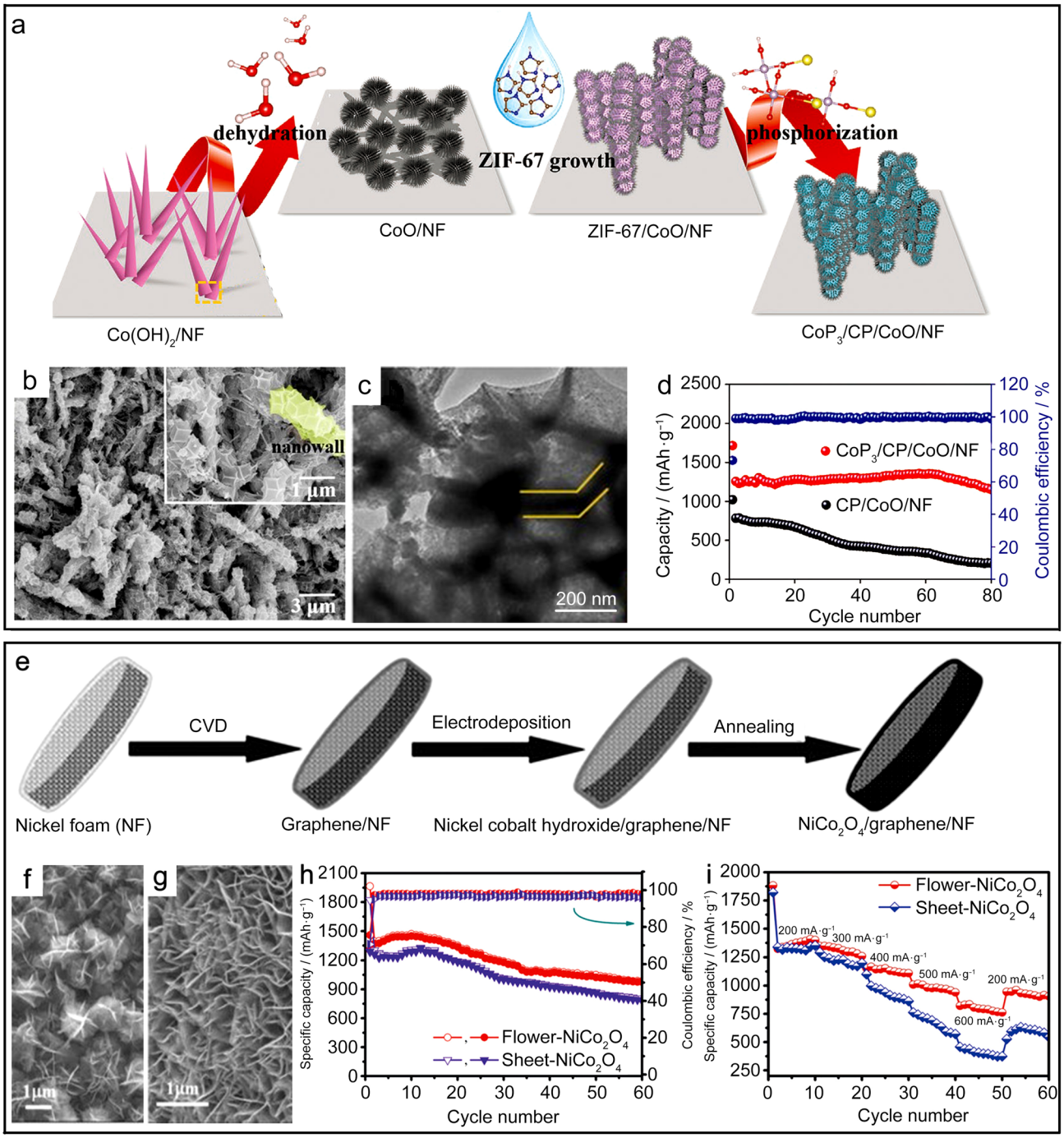

Fig. 7 **a** Preparation process, **b** SEM images, **c** HREM images and **d** rate performances of the CoP_3/CP/CoO/NF. Reproduced with permission from Ref. [74]. Copyright 2020, Wiley. **e** Schematic illustration and SEM images of **f** flower-type and **g** sheet-type $NiCo_2O_4$/3D-GNF composite. Comparison of **h** cycle and **i** rate performances for the two types $NiCo_2O_4$ in terms of discharge capacity. Reproduced with permission from Ref. [75]. Copyright 2016, Wiley

The superior rate capability of Fe_2O_3/CC can be attributed to the high conductivity and flexibility of CC, providing an efficient channel and path for the rapid electron transfer during the electrochemical processes.

Because of the high cost and toxicity of some active elements for lithium storage, more and more efforts have been devoted to partially replacing them with other cheap and environmentally friendly elements. Among them, a series of binary metal oxides such as $CuCo_2O_4$ [108–111], $MnCo_2O_4$

[112–115], $CoMn_2O_4$ [116–118], $ZnCo_2O_4$ [24, 119], $ZnMn_2O_4$ [120–123], $Co_3V_2O_8$ [124–127], and $NiCo_2O_4$ [128, 129] have also been investigated as electrode materials for LIBs. Wang et al. [130] designed the mesoporous $CoFe_2O_4$/CoO NSs assembled from the NWs precursor based on the combination of a hydrothermal synthesis of $Co_2(CO_3)(OH)_2$ NWs and a thin Fe_2O_3 coating layer on the surface of the NWs by ALD technique. With the subsequent thermal treatment, the Fe_2O_3 coated NWs partially fused together to form the NSs structure as the anode of LIBs. The as-synthesized NSs exhibit an ultra-high initial charge capacity of 1705 mAh·g^{-1} and good cycling stability (1043 mAh·g^{-1} after 50 cycles). The enhanced lithium storage performance could be ascribed to the unique structure which not only increases the electronic conductivity but also provides more active sites. Zhang et al. [75] have reported both flower- and sheet-type $NiCo_2O_4$/3D graphene-coated NF (3D-GNF) hybrids framework as a self-supported anode for LIBs. The fabrication procedure is illustrated in Fig. 7e. The subsequent electrodeposition growth of flower- (Fig. 7f) or sheet-type (Fig. 7g) spinel $NiCo_2O_4$ is carried out in a three-electrode electrolytic cell and the crystallinity of the spinel is enhanced via a subsequent annealing. Both samples exhibit high lithium storage capacity (Fig. 7h, i) where the discharge capacities are retained at 985 mAh·g^{-1} and 805 mAh·g^{-1} for flower-type and sheet-type $NiCo_2O_4$ after 60 cycles, respectively. Then, the reversible discharge capacity is 761 mAh·g^{-1} for flower-type and 374 mAh·g^{-1} for sheet-type $NiCo_2O_4$ at a current density of 600 mA·g^{-1}. Such excellent performance can be attributed to high volume utilization efficiency with unique morphological characteristics, a well-preserved connection between the active materials and the current collector, a short Li^+ diffusion path, and fast electrolyte transfer in the $NiCo_2O_4$/3D-GNF structure. The simple preparation process makes the self-supported $NiCo_2O_4$/3D-GNF hybrid a potential candidate for commercial applications.

In addition to these conversion-type lithium storage materials, there are quite some TMOs, such as titanium dioxide (TiO_2) [131–141] and vanadium oxide (VO_2) [142–147], storing lithium using the intercalation process. These electrode materials feature with relatively low theoretical specific capacities but outstanding stability.

TiO_2 has been extensively studied in recent years due to its natural abundance, low priced, environment friendliness, and long cycle life. Fan et al. [42] have fabricated the self-supported SnO_2/TiO_2 nanocomposite films with improved electrochemical performance for LIBs. SnO_2/TiO_2 nanocomposite films showed superb cycle stability (175 μAh·cm^{-2} at 13.8 μA·cm^{-2} after 200 cycles,) and high rate capability (111 μAh·cm^{-2} at 276 μA·cm^{-2}). From the ex situ field emission SEM (FESEM) observation, the cycled SnO_2/TiO_2 electrode showed less cracks on the surface of material than the pure SnO_2 anodes after 200 cycles. The improved stability benefit from the well-designed structure that can effectively mitigate the stress generated during the intercalation/deintercalation of Li^+. Moreover, the self-supported electrode was successfully used in flexible quasi-solid-state batteries and displays superior cycling stability.

VO_2 has been studied as a promising material for aqueous and nonaqueous rechargeable LIBs, owing to its proper electrode potential and tunnel structure as well as its abundant resource. There have been series of studies about VO_2 for lithium storage including various VO_2 nanostructures, [148–153] and VO_2 composites [154, 155]. Li et al. [156] have grown highly crystalline VO_2 nanobelt arrays on carbon fiber cloth (CFC) (CFC@VO_2(B)) via a facile one-pot solvothermal method successfully. Figure 8a shows a schematic illustration of the formation process which involves "self-assembly", "exfoliation" and "oriented crystallization/attachment". The as-prepared CFC@VO_2(B) nanobelt array electrodes remain stable while being folded or twisted (Fig. 8b) showing great flexibility, which also exhibit a high initial discharge capacity of 145 mAh·g^{-1} (Fig. 8c), well cycling stability with capacity retention over 90% after 200 cycles at ~ 9 °C (1000 mA·g^{-1}) (Fig. 8d), and high rate capability at high current densities up to ~ 20 °C (2000 mA·g^{-1}) (Fig. 8e). The homogenous ordered morphology of self-supported array could enhance the effective contact of the electrode and the electrolyte as well as shorten the Li^+ diffusion distance. The effective combination of CFC and a high areal mass loading of active materials is a feasible and effective solution to design high performance flexible batteries. Recent progress on self-supported TMOs-based electrodes for LIBs are summarized in Table 1, suggesting promising applications in high-performance LIBs. TMOs-based anode electrodes are, at present, mostly of academic interest until the remaining challenges will be overcome.

3.2 SIBs

SIBs as a complementary alternative to LIBs have received a great deal of attention mainly due to their low price of sodium sources. The storage of sodium also employs conversion and intercalation processes, similar to that of lithium. However, appropriate electrode materials with high capacity and excellent rate capability are still limited due to the slow ion transport, sluggish reaction kinetics, and larger volume changes during the Na^+ insertion/extraction process. Therefore, self-supported TMOs have been developed for SIBs to address the intractable issues.

CuO is an attractive candidate by virtue of its huge availability, low cost, environmental friendliness, and high theoretical capacity (674 mAh·g^{-1}). Wang et al. [161] designed high-performance SIBs based on the use of flexible membrane composed of ultrasmall TMO particles. Specifically,

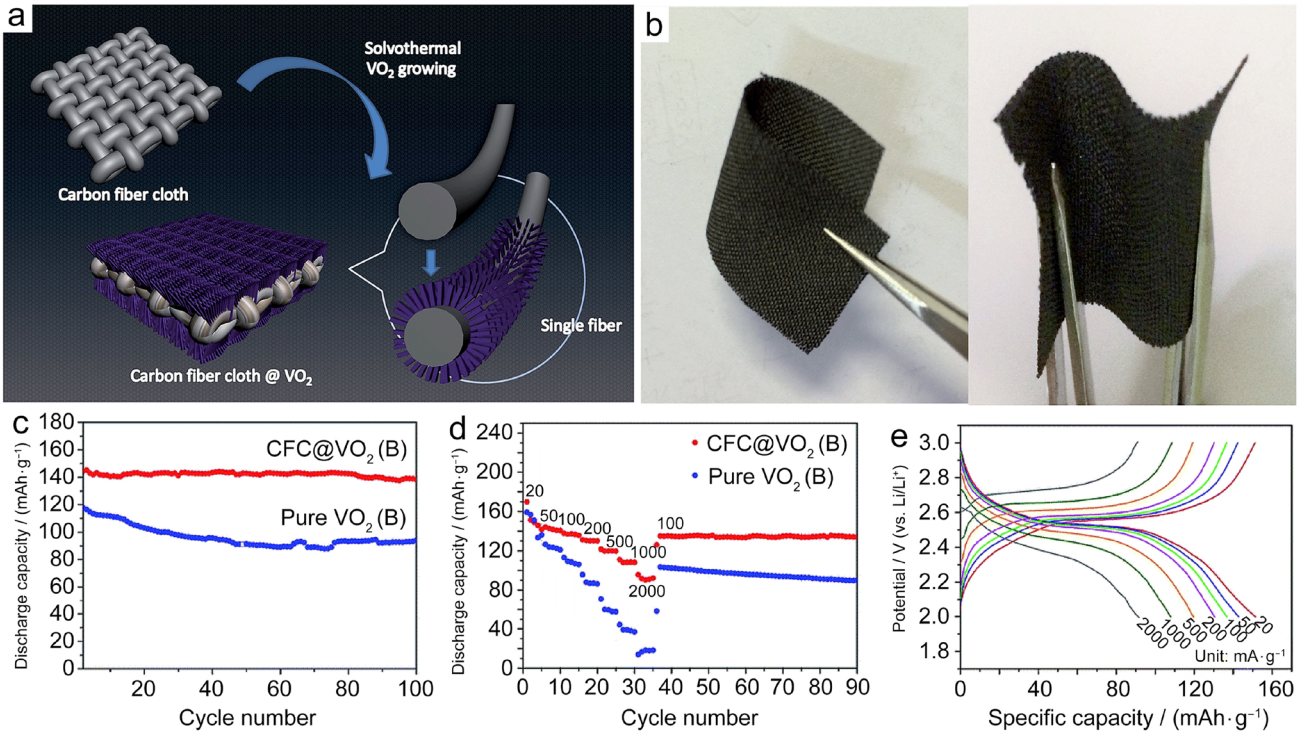

Fig. 8 **a** Schematic diagram and **b** camera image of CFC@VO_2(B) flexible cathode electrodes: folding (left), twisting (right). **c–e** Electrochemical measurements of the CFC@VO_2(B) and pure VO_2(B) cathodes. Reproduced with permission from Ref. [156]. Copyright 2016, RSC

the self-supported electrode made of CuO quantum dots uniformly encapsulated in CNFs (2-CuO@C) was constructed via a facile electrospinning method, as shown in Fig. 9a. In the SEM (Fig. 9b) and TEM (Fig. 9c) images, the CNFs are smooth and continuous with the length up to hundreds of micrometers, and the average diameter is about 80 nm, what's more, the CNFs can prevent aggregation of CuO quantum dots during the prolonged cycling process; the CuO quantum dots are delicately embedded in CNFs with the size of about 2 nm which can significantly improve the utilization rate of electrode materials. The self-supported flexible 2-CuO@C is directly used as the anode for SIBs to elucidate the electrochemical reactive processes with rapid charge and discharge, delivering a high initial reversible capacity of 528 $mAh{\cdot}g^{-1}$ at the current density of 100 $mA{\cdot}g^{-1}$ (Fig. 9d), and a high rate capability of 250 $mAh{\cdot}g^{-1}$ even at 5000 $mA{\cdot}g^{-1}$ (Fig. 9e). Such a structure could also secure excellent stability where an ultra-stable capacity of 401 $mAh{\cdot}g^{-1}$ over 500 cycles at 500 $mA{\cdot}g^{-1}$ was achieved. The simple synthesis method not only can be applied to the TMOs but also to other kinds of active materials and has great potential for practical application, especially in portable energy storage devices. Co_3O_4 is also widely used as the anode material for SIBs due to its high theoretical specific capacity. However, the poor ionic and electronic transport properties originated from the low electronic conductivity of Co_3O_4, resulted in poor cycle and rate performance. Its practical use needs to overcome the strike caused by the bigger radius of sodium ion. Liu et al. [162] reported the Co_3O_4 NPs/CNF mat anodes for SIBs, which was synthesized by a sol–gel electrospinning technique and subsequently carbonization process using poly (vinylpyrrolidone) as the carbon source. The as-prepared Co_3O_4 NPs/CNF mats demonstrated great enhancement in electrochemical performances with good rate performance and a high reversible capacity of 500 $mAh{\cdot}g^{-1}$ after 700 cycles. Electrospinning Co_3O_4 NPs/CNF mats electrodes not only take advantage of ordered ion and electronic transport path and high mechanical strain, which improve the electronic and ionic transport properties, but also its 3D network nanostructure that could prevent the aggregation of tiny NPs. Such a flexible, self-supported, and high electronic conductivity anode enables promising application for large-scale energy storage and conversion. Wang et al. [163] reported a simple preparation route to controllably fabricate self-supported structure of $CuCo_2O_4$ nanodots delicately inserted into N-doped CNFs (3-CCO@C) as an anode for SIBs. The 3-CCO@C composite exhibits high cycling stability (314 $mAh{\cdot}g^{-1}$ at 1000 $mA{\cdot}g^{-1}$ after 1000 cycles) and high rate capability (296 $mAh{\cdot}g^{-1}$ at 5000 $mA{\cdot}g^{-1}$), benefiting from the synergetic effect of ultrasmall $CuCo_2O_4$ NPs and

Table 1 Electrochemical performance of some typical self-supported TMOs electrodes for EES

Materials	Method	Reversible capacity (cycles)	Rate capacity	Energy Storage	Ref
MnO_2-rGO hybrid films on Cu foil	EPD, thermal annealing	1652.2 mAh·g^{-1} at 0.1 A·g^{-1} (200)	616.8 mAh·g^{-1} at 4 A·g^{-1}	LIBs	[34]
TiO_2/rGO nanocomposite on Cu foil	Annealing	176.0 mAh·g^{-1} at 1675 mA·g^{-1} (5000)	175.2 mAh·g^{-1} at 3350 mA·g^{-1}	LIBs	[39]
CMN-CH on Cu foil	Hydrothermal, annealing	1501 mAh·g^{-1} at 5 A·g^{-1} (1500)	823 mAh·g^{-1} at 10 A·g^{-1}	LIBs	[40]
CoO-Co nanocomposite film on Cu foil	PLD technique	830 mAh·g^{-1} at a specific current of 500 mA·g^{-1} (200)	578 mAh·g^{-1} at 10 mA·g^{-1}	LIBs	[44]
CuO/Cu hybrid foil	Wet chemical oxidation	631.6 mAh·g^{-1} at 1.0 A·g^{-1} (300)	457.7 mAh·g^{-1} at 10 A·g^{-1}	LIBs	[48]
nanocrystalline Fe_2O_3 film on Cu foil	PLD technique	905 mAh·g^{-1} at 100 mA·g^{-1} (200)	(510 mAh·g^{-1} at 15 A·g^{-1})	LIBs	[41]
CoO@C-Co foil	Nanosecond laser ablation	799.8 mAh·g^{-1} at 1.5 A·g^{-1} (800)	314.4 mAh·g^{-1} at 2 A·g^{-1}	LIBs	[49]
flower-type $NiCo_2O_4$/3D-GNF on NF	Electrodeposition	985 mAh·g^{-1} at 200 mA·g^{-1} (60)	761 mAh·g^{-1} at 600 mA·g^{-1}	LIBs	[78]
CoP_3/CP/CoO/ nanoarrays on NF	Hydrothermal, annealing	1150 mAh·g^{-1} at 0.5 A·g^{-1} after (80)	572.3 mAh·g^{-1} at 600 mA·g^{-1}	LIBs	[77]
NiO NRAs on NF	Thermal annealing	705.5 mAh·g^{-1} at 1 A·g^{-1} (70)	575 mAh·g^{-1} at 5 A·g^{-1}	LIBs	[80]
$CoFe_2O_4$/CoO NSs on NF	Hydrothermal, ALD technique	1043 mAh·g^{-1} at 358 mA·g^{-1} (50)	758 mAh·g^{-1} at 716 mA·g^{-1}	LIBs	[130]
Fe_2O_3 on SS	Magnetron sputtering deposition method	1000 mAh·g^{-1} at 400 mA·g^{-1} (100)	417.4 mAh·g^{-1} at 16 A·g^{-1}	LIBs	[56]
Co-MOF derived Co_3O_4 on Ti NWAs	Electrochemically assistant method	300 mAh·g^{-1} at 20 A·g^{-1} (200)	180 mAh·g^{-1} at 50 A·g^{-1}	LIBs	[52]
Hierarchical urchin-like Fe_2O_3 structures on Ti foil	Solvothermal, subsequent annealing	1140.3 mAh·g^{-1} at 1 A·g^{-1} (200)	900–960 mAh·g^{-1} at 5 A·g^{-1}	LIBs	[22]
TiO_2 nanotube arrays on porous Ti foam	Electrochemical anodization	101 μA·h·cm^{-2} at 10 μA· cm^{-2} (100)	83 μA·h·cm^{-2} at 500 μA· cm^{-2}	LIBs	[55]
$CuCo_2O_4$-based on NF	Hydrothermal	837 mAh·g^{-1} at 1 A·g^{-1} (250)	789 mAh·g^{-1} at 5 A·g^{-1}	LIBs	[108]
Fe_2O_3@C NRAs /CC	Hydrothermal	1635.8 mAh·g^{-1} at 0.2 A·g^{-1} (60)	384.3 mAh·g^{-1} at 2 A·g^{-1}	LIBs	[89]
3DGN/MOF-derived CuO composite	Solution immersion, thermal treatment	405 mAh·g^{-1} at 100 mA·g^{-1} (100)	219 mAh·g^{-1} at 1.6 A·g^{-1}	LIBs	[84]
CuO NWs/CFs	Electroless plating, thermal oxidation	598.2 mAh·g^{-1} at 0.1 C (50)	152.2 mAh·g^{-1} at 2 C	LIBs	[157]
Fe_2O_3/SWNT	CVD	567.1 mAh·g^{-1} at 2 A·g^{-1} (600)	384.9 mAh·g^{-1} at 5 A·g^{-1}	LIBs	[96]
$ZnCo_2O_4$/CNFs	Hydrothermal, thermal treatment	656 mAh·g^{-1} at 0.5 C (150)	225 mAh g^{-1} at 2 C	LIBs	[119]
ZnO/CNFs	Electrospinning	723 mAh·g^{-1} at 100 mA·g^{-1} (100)	1600 mAh·g^{-1} at 2 A·g^{-1}	LIBs	[158]
$MnCoO_x$@N-doped CNFs	Electrospinning	609 mAh·g^{-1} at 100 mA·g^{-1} (10)	335 mAh·g^{-1} at 1 A·g^{-1}	LIBs	[159]
ZnO@nitrogen-doped porous carbon	thermal conversion	352 mAh·g^{-1} at 1 A·g^{-1} (500)	120 mAh·g^{-1} at 8 A·g^{-1}	LIBs	[160]
CuO NSs/rGO	Vacuum filtration and hydrothermal reduction	736.8 mAh·g^{-1} at 67 mA·g^{-1} (50)	~390 mAh·g^{-1} at 3370 mA·g^{-1}	LIBs	[92]
Fe_2O_3/SnO_2 composite nanofibers	Electrospinning	850 mAh·g^{-1} at 100 mA·g^{-1} (80)	402 mAh·g^{-1} at 1.6 A·g^{-1}	LIBs	[97]
4CMC/CNT on Cu foil	Solution deposition	309 mAh·g^{-1} at 0.05 A·g^{-1} (100)	161 mAh·g^{-1} at 2 A·g^{-1}	SIBs	[36]

Table 1 (continued)

Materials	Method	Reversible capacity (cycles)	Rate capacity	Energy Storage	Ref
CuO NRAs on Cu foil	Engraved, annealing	542 mAh·g^{-1}at 50 mA·g^{-1}(30)	640 mAh·g^{-1} at 200 mA·g^{-1}	SIBs	[38]
Fe_2O_3 on SS	Electrostatic spray deposition	386 mAh·g^{-1} at 100 mA·g^{-1} (200)	233 mAh·g^{-1} at 5 A·g^{-1}	SIBs	[57]
2-CuO@C	Electrospinning	440 mAh·g^{-1} at 100 mA·g^{-1} (100)	246 mAh·g^{-1} at 5 A·g^{-1}	SIBs	[161]
Co_3O_4 NPs /carbon composite nanofiber	Sol–gel electrospinning	500 mAh·g^{-1} (700)	75 mAh·g^{-1} at 1 C	SIBs	[162]
N-Doped $CuCo_2O_4$@C Film	Electrospinning	314 mAh·g^{-1} at 1000 mA·g^{-1} (1000)	296 mAh·g^{-1} at 5 A·g^{-1}	SIBs	[163]
BT/CNFs	Electrospinning, alkali hydrothermal treatment	283.5 mAh·g^{-1} at 200 mA·g^{-1} (1000)	204.2 mAh·g^{-1} at 2 A·g^{-1}	SIBs	[94]
$MnCo_2O_4$ NWs bundles on NF	Hydrothermal	1000 mAh·g^{-1} at 0.1 mA·cm^{-2} (144)	4771 mAh·g^{-1} at 1 mA·cm^{-2}	Li-O_2	[68]
Co_3O_4/CNFs	Electrospinning, thermal treatment	418 mAh·g^{-1} at 500 mA·g^{-1} (10)	–	Li-O_2	[164]
Co-Mn thin film composite oxide	Electrolytic	2000 mAh·g^{-1} at a current of 0.1 mA·cm^{-2} (multiple)	–	Li-O_2	[165]
Co_3O_4 films on NF	Electrochemical deposition	1000 mAh·g^{-1} at 0.2 A·g^{-1} (35)	416 mAh·g^{-1} at 0.5 A·g^{-1}	Li-O_2	[72]
$FeCo_2O_4$ NSs on NF	Hydrothermal	7733 mAh·g^{-1} at 0.2 A·g^{-1} (–)	6024 mAh·g^{-1} at 0.4 A·g^{-1}	Li-O_2	[70]
NS@$Co_{3-x}Ni_xO_4$/Co_3O_4	Hydrothermal	200 cycles over 8 days at 5 mA·cm^{-2}	-	Zn-O_2	[51]
TiO_{2-x}/CNTs	Hydrothermal	104 Wh·kg^{-1} at 250 W·kg^{-1}	32 Wh·kg^{-1} at 5 kW·kg^{-1}	LICs	[95]
TiO_{2-x}/CNTs	Hydrothermal	109 Wh·kg^{-1} at 250 W·kg^{-1}	36 Wh·kg^{-1} at 5 kW·kg^{-1}	SICs	[95]
CNTs@MnO_2 on NF	CVD, hydrothermal	208 F·g^{-1} at 10 A·g^{-1} (5000)	230 F·g^{-1} at 10 A·g^{-1}	SCs	[166]
Co_3O_4 wire-penetrated-cage hybrid NWAs on NF	Annealing	2.8 F·cm^{-2} at 10 mA·cm^{-2} (12,000)	2.8 F·cm^{-2} at 20 mA·cm^{-2}	SCs	[76]
Ni-G-CNFs@polyaniline throns	Electrospinning, carbonization	Capacitance retention of 85.8% at 1 A·g^{-1} (1000)	14.4 Wh·kg^{-1} at 375.2 W·kg^{-1}	SCs	[167]
$ZnCo_2O_4$-rGO on NF	Hydrothermal, thermal annealing	3222 F·g^{-1} at 1 A·g^{-1} (–)	860 F·g^{-1} at 20 A·g^{-1}	SCs	[168]
$NiCo_2O_4$@$NiWO_4$ core–shell NWAs on NF	Hydrothermal, thermal treatment	Capacitance retention of 87.6% at 5 A g^{-1} (6000)	1384 F·g^{-1} at 1 A·g^{-1}	SCs	[169]
MnO_2 on foamed-Ni	Hydrothermal	2.31 F·cm^{-2} at 1 mA·cm^{-2} (–)	1.48 F·cm^{-2} at 20 mA·cm^{-2}	SCs	[65]
$NiCo_2O_4$ NSs on CC	Hydrothermal	183.1 mAh·g^{-1} at 1.6 A·g^{-1} (–)	96.1 mAh·g^{-1} at 32 A·g^{-1}	Ni//Zn batteries	[85]

N-doped carbon matrix which can improve the utilization rate, and thus increase the real specific capacity.

TiO_2 based materials are also capable of sodium storage but their performance is largely retarded by the intrinsic low electric conductivity and sluggish diffusion of sodium ions [170–174]. Constructing self-supported electrodes has been demonstrated as an appealing approach to address these intrinsic drawbacks [45, 55, 175]. Wang et al. [94] reported a rational design of free-standing BT/C NFs and the preparation method is described in detail in Fig. 9d. After 1000 cycles, a high discharge capacity of 283.5 mAh·g^{-1} at a current density of 200 mA·g^{-1} can be still achieved (Fig. 9f). Even at a high current density of 2 A·g^{-1}, the reversible capacity as high as 204 mA·h·g^{-1} can still be achieved (Fig. 9g). The high rate performance is mainly due to the capacitive-controlled process instead of diffusion-dominated sodium storage. Figure 9h shows that the proportion of the pseudocapacitive contribution gradually increased from 70.8% to 88.3% with the increase of scan rates. This result revealed that the majority of the capacity originated from surface pseudocapacitive behavior, which strengthened the Na^+ insertion/extraction and guaranteed its excellent electrochemical performance. The self-supported hierarchically branched TiO_2/C nanofibers with the inherent

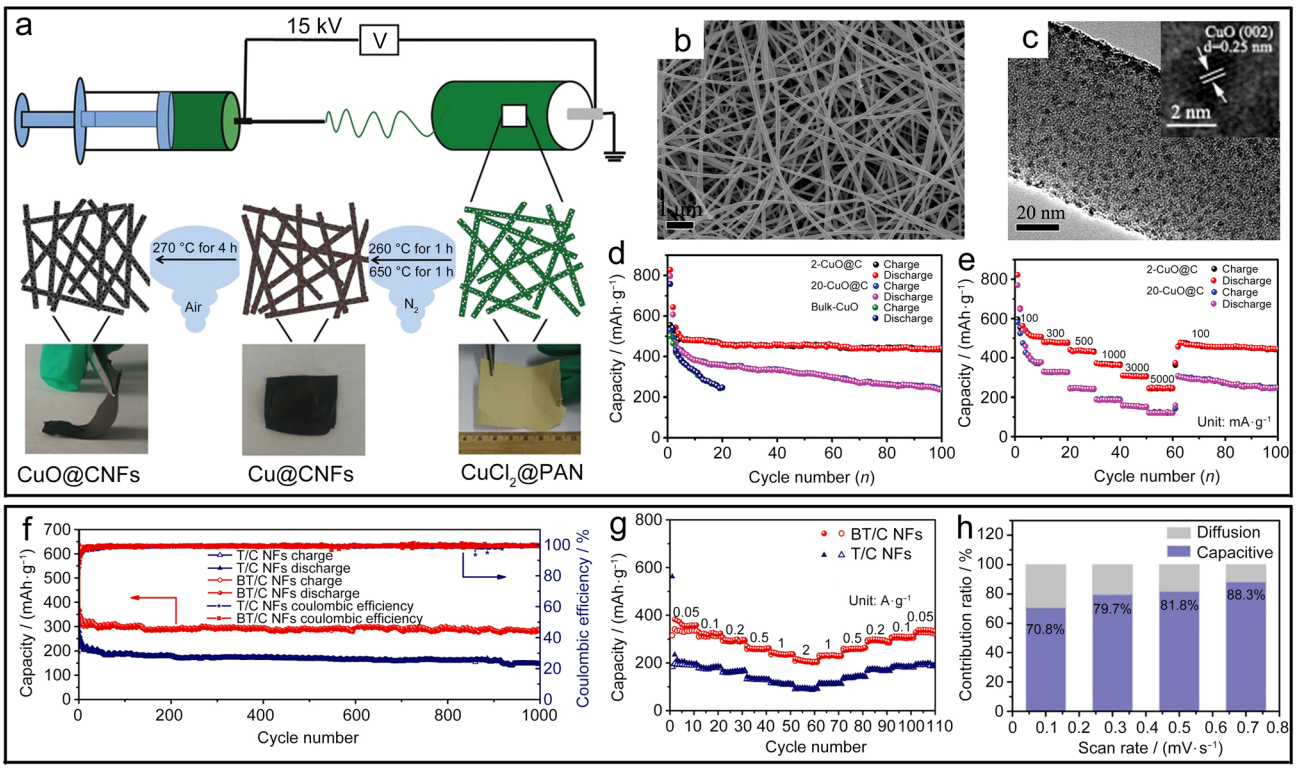

Fig. 9 **a** Illustration of the formation process for CuO@C nanofibers, **b** SEM and **c** TEM images of 2-CuO@C (inset: corresponding HRTEM images), **d** cycling performances and **e** rate capability of electrode samples. Reproduced with permission from Ref. [161]. Copyright 2016, Wiley. **f** Cycling performance, **g** rate performance and **h** contribution ratios of capacitance- and diffusion-controlled processes at different scan rates of BT/C NFs. Reproduced with permission from Ref. [94]. Copyright 2019, Wiley

pseudocapacitive endow this material with promising potential for SIBs and some other flexible electronic devices. Table 1 presents the recent progress of self-supported TMOs as electrode materials for high-performance SIBs. However, there are still some huge challenges for SIBs, including low reversible capacity, unsatisfied Coulombic efficiency and high operating voltage.

3.3 Other batteries

With the large deployment of renewable energy, electrochemical energy storage systems will be of paramount importance and the current LIBs and SIBs cannot fulfill all the requirements for the emerging applications. Therefore, some novel batteries, such as AIBs, metal-air batteries, etc., have been developed [176–178].

Al is an abundant, recyclable, environmentally friendly metal and it is much cheaper than that of most other metals used for electrochemical energy storage. Al is attractive as the anode because it has a relatively low standard reduction potential. Most significantly, the high material density (2.70 $cm^3 \cdot g^{-1}$) of Al leads to an ultra-high volumetric capacity of around 8046 $mAh \cdot cm^{-3}$, which is four times higher than that of lithium (2062 $mAh \cdot cm^{-3}$) [179–182]. Over the past few years, a series of materials such as Co_3O_4@MWCNTs [183], bronze-type VO_2 holey nanobelts [184], TiO_2 nanospheres [185], and TMO NPs@rGO [186] have been explored to pair with the Al foil for AIBs. Due to the high charge density of the Al^{3+}, it could be difficult for Al ions to intercalate into the framework of the active materials [11, 15]. In principle, a suitable intercalation cathode needs a large 2D and/or 3D framework and wide insertion/extraction channel to stably accommodate Al ions. Chattopadhyay and his colleagues reported the direct growth of nanoscale ZnO on SS through ALD technique (ZnO ALD-E) for Al storage [187]. The surface morphology indicates the formation of typically uniform, dense, homogeneous, pinhole-free, and smooth ZnO film conformal to the underlying substrate (Fig. 10a, b). ZnO ALD-E shows high electrochemical performance as a self-supported cathode for AIBs which manifests an initial discharge/charge capacity is 2563 and 1639 $mAh \cdot g^{-1}$ (Fig. 10c), and remains at 245 $mAh \cdot g^{-1}$ at a current rate of 400 $mA \cdot g^{-1}$ after 50 cycles (Fig. 10d). More importantly, the discharge capacity of the battery with self-supported ZnO-ALD-E cathode is significantly higher than that of batteries fabricated using a conventional slurry-casting ZnO cathode.

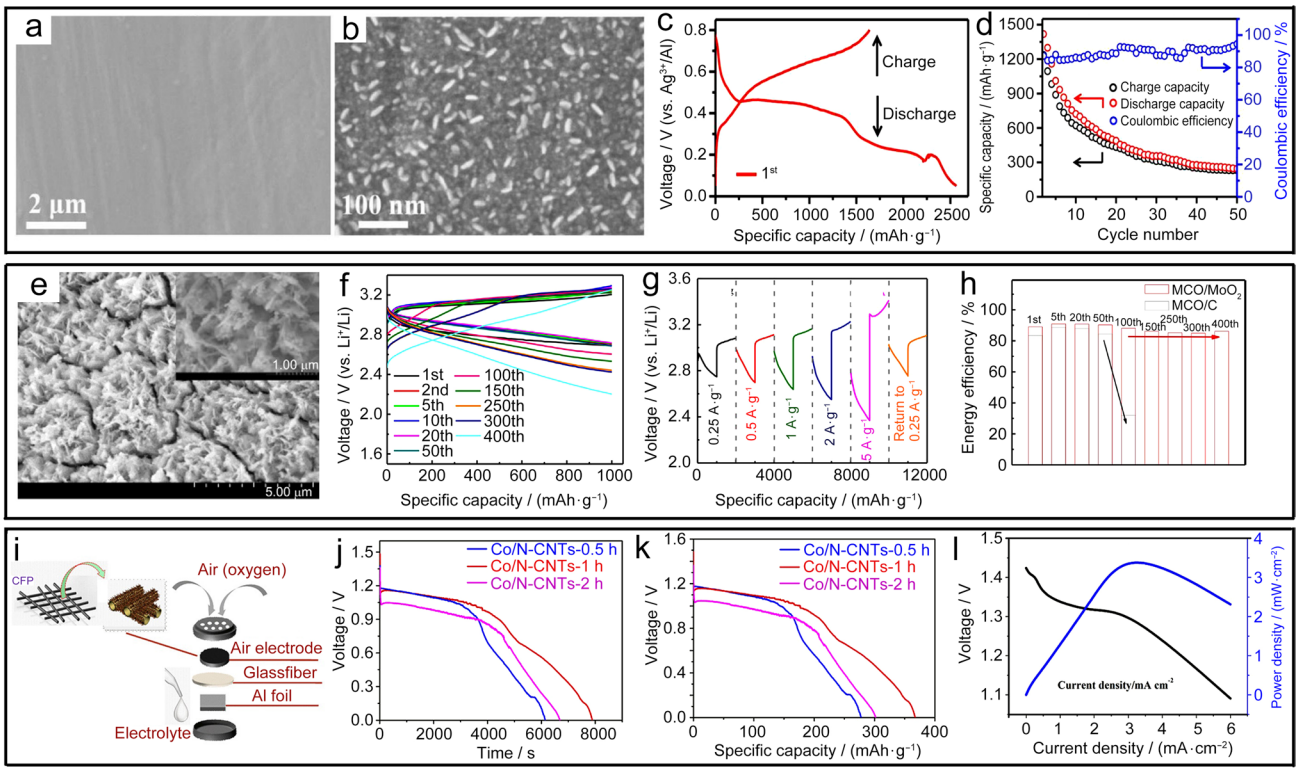

Fig. 10 **a**, **b** FESEM image of ZnO-ALD-E. **c** Initial discharge/charge curves and **d** cycle performance of Al/ZnO-ALD-E batteries. Reproduced with permission from Ref. [187]. Copyright 2018, Wiley. **e** SEM images MCO/MoO_2@Ni (inset: HRSEM). Electrochemical characterizations of MCO/MoO_2@Ni cathode for Li-O_2 batteries: **f** Cycling performance, **g** rate performances and **h** energy efficiency of MCO/MoO_2@Ni and MCO/C@Ni cathode. Reproduced with permission from Ref. [190]. Copyright 2018, Wiley. **i** Configuration of an Al-air coin cell. **j** Voltage–time, **k** voltage-specific capacity and **l** power–current density curves for Co@CoO_x/HNCNTs-1 h. Reproduced with permission from Ref. [90]. Copyright 2020, ACS

The rechargeable metal-air batteries are attractive because of their ultra-high theoretical energy density among the existing EES systems. The reaction principle of metal-air batteries includes the oxygen reduction reaction (ORR) and oxygen evolution reaction (OER) on the air electrode, which correspondingly involves the formation and decomposition of metal peroxide during the discharge and charge processes, respectively. However, the carbon-based materials which is a promising candidate for the air electrode will produce metal oxides that could react with carbon to form an insulating metal carbonate layer during the discharge process, resulting in cathode passivation and capacity fading in metal-air batteries. These problems can be circumvented by replacing carbon with self-supported electrodes, where the performance of these electrodes based on Co_3O_4 [164, 188], MnO_2 [107], and NiO [189] have been reported. For example, $MnCo_2O_4$ NPs anchored on porous MoO_2 NSs that are grown on NF (MCO/MoO_2@Ni) we synthesized successfully by Cao et al. [190] acting as a cathode for Li-O_2 batteries directly. $MnCo_2O_4$ possesses spinel structure which has been reported to be efficient electrocatalysts for the cathode of Li-O_2 batteries owing to the variable valence states of Mn and Co. MoO_2 shows a metallic conductivity with a low resistivity and high chemical stability and the sheet-like structure can facilitate the oxygen diffusion, transport of electrolyte, and deposition of discharge products. Moreover, MCO/MoO_2 directly grown on NF ensured the low interfacial resistance between the catalyst and the current collector. The thickness of the MoO_2 NSs is around 20 nm and the average size of MCO NPs is 30 nm (Fig. 10e). This MCO/MoO_2@Ni electrode delivers excellent cyclability (more than 400 cycles, Fig. 10f) and rate performance (Fig. 10g). Notably, the battery with this electrode exhibits a high energy efficiency (higher than 85%, Fig. 10h). The long life and high Coulombic efficiency of the MCO/MoO_2@Ni cathode could be attributed to the improved electrical conductivity, efficient oxygen diffusion and electrolyte transport, effective O_2/Li_2O_2 conversion, and the synergistic combination of MCO and MoO_2. Moreover, Jiang et al. [68] obtained a hierarchically porous three-dimensional $MnCo_2O_4$ nanowire bundles electrodes for Li-O_2 cell showing a high discharge capacity of up to 12,919 mAh·g^{-1} at 0.1 mA·cm^{-2} and excellent rate capability. Even under constrained specific capacities of 500 and 1000 mAh·g^{-1}, Li-O_2 batteries

could be successfully operated for over 300 and 144 cycles, respectively. Their excellent electrochemical performance is proposed to be related to the conductivity enhancements resulting from the hierarchical interconnected mesoporous/macroporous web-like structure of the hybrid $MnCo_2O_4$ cathode, which facilitated the electron and mass transport. Liu et al. [90] synthesized high-purity Co@CoO_x/helical nitrogen doped CNTs (Co@CoO_x/HNCNTs) on carbon fiber papers, and used them as self-supported cathodes for Al-O_2 batteries. The configuration of an Al-air coin cell employing Co@CoO_x/HNCNTs-1 h as the self-supported cathode is shown in Fig. 10i, which exhibits an open circuit voltage of 1.48 V (Fig. 10j), a specific capacity of 367.31 mAh·g^{-1} at the discharge current density of 1.0 mA·cm^{-2} (Fig. 10k), and a maximum power density of 3.86 mW·cm^{-2} (Fig. 10l). This work not only proposes an innovative and general strategy for preparing high-purity Co@CoO_x/HNCNTs, but also provides valuable guidance for designing and developing Co@CoO_x/HNCNTs as self-supported electrodes in the Al-O_2 battery, which can be further extended to be used in various metal-air systems. The recent progress of self-supported TMOs in LICs, SICs, Li-O_2, and etc. is summarized and presented in Table 1.

3.4 Supercapacitors

Electrochemical capacitors (or SCs) have been deemed to be one of the most promising powerful EES devices, owing to long cycle lives, high power densities, and fast rate capabilities. Depending on their mechanisms for energy storage, SCs can be divided into two types, namely electrical double layer capacitors (EDLCs) and pseudo-capacitors. EDLCs are characterized by the electrostatic adsorption of ions at the electrode/electrolyte interface and the ordinary electrode materials are carbon-based materials, such as AC [191–193], graphene [194, 195], and porous carbon [196–198], presenting high surface areas, good electronic conductivities, and chemical stabilities. Pseudo-capacitors are based on rapid and reversible faradaic charge transfer with an oxidation/reduction (redox) and/or ion-intercalation process, which could offer substantially higher specific capacitance and energy density than typical EDLCs. The active materials in the electroactive species contain hydroxides, TMOs, and conducting polymers, among them, offering the specific capacitances one order of magnitude higher than that of EDLCs [199–203].

Li et al. [62] reported a series of self-supported electrodes with hierarchical manganese dioxide NSs anchoring on Ni frameworks (Ni/MnO_2) by a hydrothermal method for SCs. Such hierarchical NSs of MnO_2 can improve its electrolyte-accessible surface area and the NF can effectively enhance its electronic conductivity. The Ni/MnO_2-9 electrode reveals the highest areal specific capacitance of 2.31 F·cm^{-2} at a current density of 1 mA·cm^{-2} among these electrodes, which can maintain 1.48 F·cm^{-2} (64.1%) at 20 mA·cm^{-2}, implying excellent rate capability. Furthermore, the Ni/MnO_2-9 electrode-based SC exhibits a superior energy density of 160.1 mWh·cm^{-2}, as well as an outstanding cycling stability with 86.8% capacitance retention of the initial capacitance after 9000 cycles. Pan et al. [204] reported a facile method to construct a nanoporous Ni architecture on the surfaces of CC (Ni@CC). By electrodeposition of ultrathin MnO_x NSs on the 3D Ni@CC nanoporous (3D MnO_x@Ni@CC) current collectors, an areal specific capacitance of 906.6 mF·cm^{-2} at 1 mA·cm^{-2} was achieved. Except for monometallic oxides, bimetallic metal oxides such as $NiCo_2O_4$ [205–208], $NiMoO_4$ [209–211], $MnCo_2O_4$ [212–214], and $CuCo_2O_4$ [215], have been intensively studied. However, the large-scale practical application of bimetallic oxides in SCs is still restricted by their low energy density, poor rate capability and cycling performance. To obtain electrodes for high-performance SCs, an effective approach is directly growing electroactive materials on various highly conductive substrates such as $NiCo_2S_4$@$NiMoO_4$ core–shell NSs on NF [216], $NiCo_2O_4$ on NF [169, 217–219], $NiMoO_4$ NWs on CC [220], porous $NiCo_2O_4$ NSs on carbon fabric [221].

Qu et al. [222] reported the construction of modified CNFs with multiple carbonized channels wrapped by $NiCo_2O_4$ NSs ($NiCo_2O_4$/MCMF) through CVD, the schematic illustration of the preparation process is shown in Fig. 11a. It is found in the SEM images that all the carbonized channels in $NiCo_2O_4$/MCMF are uniformly wrapped by $NiCo_2O_4$ NSs (Fig. 11b) which can offer abundant redox active sites for pseudocapacitive reaction and numerous accommodation sites for charge storage. The resultant $NiCo_2O_4$/MCMF also shows acceptable mechanical stability to endure external force and small electrical resistance. Profiting from the unique architecture, the $NiCo_2O_4$/MCMF electrode exhibits excellent specific capacitance [1541 F·g^{-1} at 1 A·g^{-1} and 1120 F·g^{-1} at 20 A·g^{-1}, (Fig. 11c)] with strong durability [85.8% capacitance retention after 10,000 cycles at 10 A·g^{-1}, (Fig. 11d)]. Furthermore, the asymmetric SCs (ASCs) with high performance were assembled using $NiCo_2O_4$/MCMF as the positive electrode and MCMF as the negative electrode. The ASCs exhibit low internal resistance, a large energy density (53.1 Wh·kg^{-1}) and high power density (18,000 W·kg^{-1}) (Fig. 11e), which can act as efficient energy storage devices to supply power without obvious degradation over repeated cycles.

$ZnCo_2O_4$-rGO composites prepared by Gao et al. [168] were deposited on the NF substrate through micelles modulated hydrothermal deposition and subsequent annealing treatment to entangle the intertwined NSs with vertical macroporous channels (Fig. 11f, g). The variable valences of Zn, Co elements also endow $ZnCo_2O_4$ with high redox activity, therefore can offer high specific capacitance. Hence,

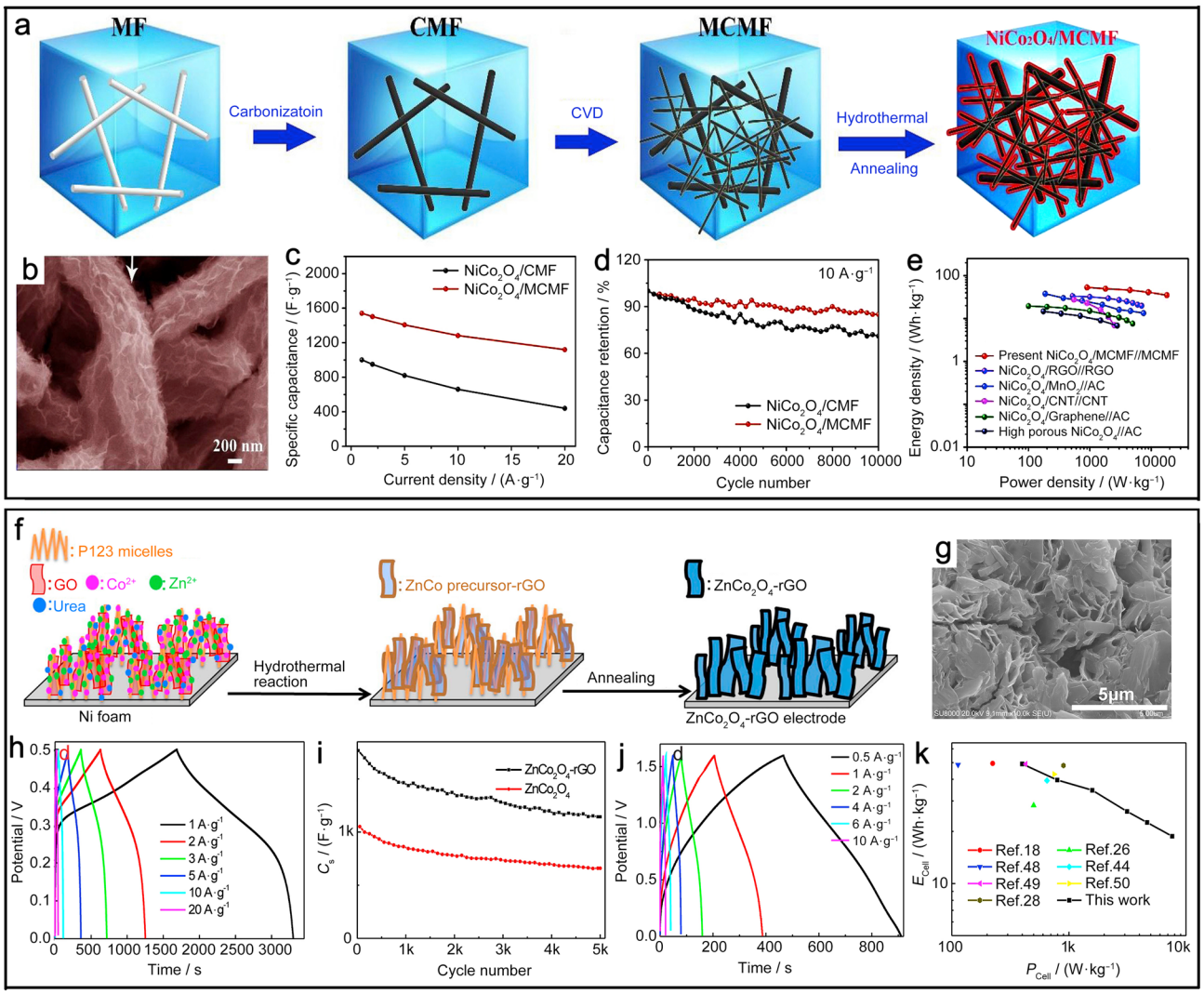

Fig. 11 **a** Illustration of the preparation process, **b** SEM images, **c** rate capability and **d** cycle stability of $NiCo_2O_4$/MCMF composite electrodes; **e** ragone plots of $NiCo_2O_4$/MCMF composite and the reported ASCs with $NiCo_2O_4$-derived electrode materials. Reproduced with permission from Ref. [222]. Copyright 2019, Elsevier. **f** Schematic illustration on the preparation process, **g** SEM images, and **h** GCD curves of $ZnCo_2O_4$-rGO composite electrode; **i** cycle abilities of $ZnCo_2O_4$-rGO and $ZnCo_2O_4$ electrodes, **j** GCDs at different current densities and **k** cycle ability of the asymmetric $ZnCo_2O_4$-rGO// AC SC. Reproduced with permission from Ref. [168]. Copyright 2018, Elsevier

$ZnCo_2O_4$ with different architectures were widely designed as efficient faradic electrodes of supercapacitors. In Gao's report, the porous $ZnCo_2O_4$-rGO electrode could offer an ultrahigh specific capacitance of 3222 $F{\cdot}g^{-1}$ at 1 $A{\cdot}g^{-1}$ in an alkali electrolyte, the specific capacitance still retains to be 860 $F{\cdot}g^{-1}$ at 20 $A{\cdot}g^{-1}$ (Fig. 11h) and exhibits good cycle ability (Fig. 11i). Moreover, when used as positive electrode of a full cell, the $ZnCo_2O_4$-rGO//AC ASC delivers a maximum specific capacitance of 139 $F{\cdot}g^{-1}$ at 0.5 $A{\cdot}g^{-1}$ (Fig. 11j) and therefore an energy density of 49.1 $Wh{\cdot}kg^{-1}$ at power density of 400 $W{\cdot}kg^{-1}$ (Fig. 11k). More significantly, ASC also exhibits excellent cycle stability with only 6% of the specific capacitance fade after 5000 continuous charge and discharge cycles. The balanced energy density, power density, and high cycle ability highlight the potential of the faradic $ZnCo_2O_4$-rGO composite in high performance and long lifetime energy storage devices. TMOs-based electrode materials have shown excellent performance and great potential in increasing both the energy density and the power density. As research goes further, light SCs with high energy density will be realized in the near future, which will play an important role in the field of energy storage.

4 Summary and prospects

In this review, we have systematically summarized the recent progress in self-supported TMOs electrodes from two aspects: synthesizing strategies and their applications in EES system. From the viewpoint of controlled syntheses, the method of synthesizing self-supported electrodes can be mainly divided into the in-situ growth of active species on the current collectors and the assembly of active materials with conductive materials into free-standing architectures via various methods such as PLD, CVD, hydrothermal, annealing, electrospinning, solvothermal, etc. In terms of in-situ growth methods, various substrates such as metal foil substrates (Cu foil, Co foil, NF, and SS etc.), porous metal substrates and carbonaceous substrates (CC, CFP, and CNFs etc.) are used to construct self-supported electrodes. The assembly methods mainly include electrospinning method which combined active materials with carbon-based materials. On the other hand, we also enumerated different energy storage applications including LIBs, SIBs, AIBs, metal-air batteries as well as SCs.

Self-supported TMOs electrodes provide great opportunity for high-performance energy storage devices in terms of their high charge transfer efficiency, and structural stability. The comparison of some typical materials, synthesis methods, and electrochemical performance of different kinds of self-supported electrodes for distinct storage systems are summarized in Table 1. As mentioned in this report, self-supported TMOs electrodes have exhibited outstanding electrochemical performance, achieved significant achievements and shown a great promise in the field of EES. Different electrode materials have their own advantages and shortcoming. For example, carbon-based materials have good cycling stability while their low capacity is deleterious for practical applications. Therefore, more effective strategies are needed to improve the performance of self-supported TMOs electrodes-based EES devices. Further improvements could be made from the following aspects.

1. Metal-based substrates are usually used to prepare nanoarray electrodes. These integrated electrodes have large specific surface area, oriented electronic and ionic transport path, and good electrical conductivity. However, most of them contain high content of auxiliary materials which inevitably reduce the energy density. Additionally, the close contact between the substrates and the nanoarrays is very important for the stability of the EES devices, thus the proper surface treatment of the substrates and the optimization of electrode preparation are highly needed.
2. The preparations of in-situ growth TMOs electrodes still have some disadvantages compared with assembled electrodes. It is urgent to simplify the preparation process and reduce the non-electroactive species weight in the whole electrodes for their further applications.
3. Self-supported TMOs electrodes exhibit excellent electrochemical properties due to the excellent electrical conductivity and reduced size of active species. It is worth noting that the TMOs content in the composites and the size of the active particles are very crucial for the conductivity and ion diffusion of EES.
4. Because of the complicated reaction mechanisms and less researches of TMOs, we still can't understand them in detail. Although great progress has been achieved already through some researchers' work, the definite origin of the voltage hysteresis is still unclear in the electrochemical reaction. Apart from this, it's very important to further study the complex mechanisms which can explain the binary TMOs reaction progress even with two storage mechanisms. This requires collaborative efforts of chemists, physicists and other fields' researchers.

Self-supported TMOs electrodes not only exhibit their superiority in the field of EES but also are expected to develop their advantages in the field of catalysis. The self-supported catalysts by directly growing the active material on a current collector is considered to be an efficient strategy to expose more active sites, promote diffusion, increase electron transfer resistance and then improve catalytic activity. Therefore, we firmly believe that the self-supported electrodes have bright application prospects in the field of energy storage and catalysis.

Acknowledgements This work was finally supported by the National Nature Science Foundation of China (Grant No. 21975287), the start-up funding support of China University of Petroleum (East China), Taishan Scholar Project (Grant No. ts201712020), Technological Leading Scholar of 10000 Talent Project (Grant No. W03020508), Shandong Provincial Natural Science Foundation (Grant No. ZR2018ZC1458).

References

1. Gong J, Li C, Wasielewski MR. Advances in solar energy conversion. Chem Soc Rev. 2019;48(7):1862.
2. Li Q, Liu Y, Guo S, Zhou H. Solar energy storage in the rechargeable batteries. Nano Today. 2017;16:46.
3. Ma Q, Wang P. Underground solar energy storage via energy piles. Appl Energy. 2020;261:114361.
4. Shoaib M, Siddiqui I, Rehman S, Khan S, Alhems LM. Assessment of wind energy potential using wind energy conversion system. J Clean Prod. 2019;216:346.
5. Bechtle P, Schelbergen M, Schmehl R, Zillmann U, Watson S. Airborne wind energy resource analysis. Renew Energ. 2019;141:1103.

6. Javed MS, Zhong D, Ma T, Song A, Ahmed S. Hybrid pumped hydro and battery storage for renewable energy based power supply system. Appl Energ. 2020;257:114026.
7. Kocaman AS, Modi V. Value of pumped hydro storage in a hybrid energy generation and allocation system. Appl Energ. 2017;205:1202.
8. Li H, Zhang X, Zhao Z, Hu Z, Liu X, Yu G. Flexible sodium-ion based energy storage devices: recent progress and challenges. Energy Storage Mater. 2020;26:83.
9. Maleki K, Sari H, Li X. Controllable cathode-electrolyte interface of $Li[Ni_{0.8}Co_{0.1}Mn_{0.1}]O_2$ for lithium ion batteries: a review. Adv Energy Mater. 2019;9(39):1901597.
10. Liu Y, Wu Q, Liu L, Manasa P, Kang L, Ran F. Vanadium nitride for aqueous supercapacitors: a topic review. J Mater Chem A. 2020;8(17):8218.
11. Yang Z, Tian J, Yin Z, Cui C, Qian W, Wei F. Carbon nanotube- and graphene-based nanomaterials and applications in high-voltage supercapacitor: a review. Carbon. 2019;141:467.
12. Ellis BL, Knauth P, Djenizian T. Three-dimensional self-supported metal oxides for advanced energy storage. Adv Mater. 2014;26(21):3368.
13. Wang H, He J, Liu J, Qi S, Wu M, Wen J, Chen Y, Feng Y, Ma J. Electrolytes enriched by crown ethers for lithium metal batteries. Adv Funct Mater. 2020;1:2002578.
14. Qi S, Wang H, He J, Liu J, Cui C, Wu M, Li F, Feng Y, Ma J. Electrolytes enriched by potassium perfluorinated sulfonates for lithium metal batteries. Sci Bull. 2020. https://doi.org/10.1016/j.scib.2020.09.018.
15. Xu C, Yang Y, Wang H, Xu B, Li Y, Tan R, Duan X, Wu D, Zhou M, Ma J, Xu B. Roadmap on electrolytes for lithium- and sodium-metal batteries. Chem Asian J. 2020. https://doi.org/10.1002/asia.202000851.
16. Fang S, Bresser D, Passerini S. Transition metal oxide anodes for electrochemical energy storage in lithium- and sodium-ion batteries. Adv Energy Mater. 2019;10(1):1902485.
17. Zhang Y, Zhang L, Lv T, Chu PK, Huo K. Two-dimensional transition metal chalcogenides for alkali metal ions storage. Chemsuschem. 2020;13(6):1114.
18. Liu Q, Hu Z, Chen M, Zou C, Jin H, Wang S, Chou S, Dou S. Recent progress of layered transition metal oxide cathodes for sodium-ion batteries. Small. 2019;15(32):e1805381.
19. Yin D, Huang G, Na Z, Wang X, Li Q, Wang L. CuO nanorod arrays formed directly on Cu foil from MOFs as superior binder-free anode material for lithium-ion batteries. ACS Energy Lett. 2017;2(7):1564.
20. Xia T, Wang Y, Mai C, Pan G, Zhang L, Zhao W, Zhang J. Facile in situ growth of ZnO nanosheets standing on Ni foam as binder-free anodes for lithium ion batteries. RSC Adv. 2019;9(34):19253.
21. Li R, Huang J, Li J, Cao L, Luo Y, He Y, Lu G, Yu A, Chen S. Nitrogen-doped hard carbon on nickel foam as free-standing anodes for high-performance sodium-ion batteries. ChemElectroChem. 2019;7(3):604.
22. Cao Y, Zhang A, Luo H, Gao H, Yan J, Yan Q, Liu Y, Zhang Y. Hierarchical urchin-like Fe_2O_3 structures grown directly on Ti foils for binder-free lithium-ion batteries with fast charging/discharging properties. Inorg Chem Commun. 2020;113:107769.
23. Sun M, Wang Z, Ni J, Li L. Dual-doped hematite nanorod arrays on carbon cloth as a robust and flexible sodium anode. Adv Funct Mater. 2020;30(11):1910043.
24. Liu T, Wang W, Yi M, Chen Q, Xu C, Cai D, Zhan H. Metal-organic framework derived porous ternary $ZnCo_2O_4$ nanoplate arrays grown on carbon cloth as binder-free electrodes for lithium-ion batteries. Chem Eng J. 2018;354:454.
25. Khan Z, Park S, Hwang SM, Yang J, Lee Y, Song H, Kim Y, Ko H. Hierarchical urchin-shaped α-MnO_2 on graphene-coated carbon microfibers: a binder-free electrode for rechargeable aqueous Na-air battery. NPG Asia Mater. 2016;8(7):e294.
26. Zhang Z, Tan Q, Zhong Z, Su F. High-performance nickel manganese ferrite/oxidized graphene composites as flexible and binder-free anodes for Li-ion batteries. RSC Adv. 2015;5(50):40018.
27. Jin T, Han Q, Jiao L. Binder-free electrodes for advanced sodium-ion batteries. Adv Mater. 2020;32(3):e1806304.
28. Shobana MK. Self-supported materials for battery technology–a review. J Alloy Compd. 2020;831:154844.
29. Pan J, Tian X, Zaman S, Dong Z, Liu H, Park HS, Xia B. Recent progress on transition metal oxides as bifunctional catalysts for lithium-air and zinc-air batteries. Batt Supercaps. 2018;2(4):336.
30. Boyd S, Augustyn V. Transition metal oxides for aqueous sodium-ion electrochemical energy storage. Inorg Chem Front. 2018;5(5):999.
31. Clément RJ, Lun Z, Ceder G. Cation-disordered rocksalt transition metal oxides and oxyfluorides for high energy lithium-ion cathodes. Energ Environ Sci. 2020;13(2):345.
32. Low WH, Khiew PS, Lim SS, Siong CW, Ezeigwe ER. Recent development of mixed transition metal oxide and graphene/mixed transition metal oxide based hybrid nanostructures for advanced supercapacitors. J Alloy Compd. 2019;775:1324.
33. Li Q, Li H, Xia Q, Hu Z, Zhu Y, Yan S, Ge C, Zhang Q, Wang X, Shang X, Fan S, Long Y, Gu L, Miao G, Yu G, Moodera JS. Extra storage capacity in transition metal oxide lithium-ion batteries revealed by in situ magnetometry. Nat Mater. 2020. https://doi.org/10.1038/s41563-020-0756-y.
34. Xu T, Meng Q, Fan Q, Yang M, Zhi W, Cao B. Electrophoretic deposition of binder-free MnO_2/graphene films for lithium-ion batteries. Chinese J Chem. 2017;35(10):1575.
35. Huang XL, Wang RZ, Xu D, Wang ZL, Wang HG, Xu JJ, Wu Z, Liu QC, Zhang Y, Zhang XB. Homogeneous CoO on graphene for binder-free and ultralong-life lithium ion batteries. Adv Func Mater. 2013;23(35):4345.
36. Miao S, Zhao H, Kang M, Shen H, Song W, Zhao D, Ye J, Li Z. High gravimetric and volumetric sodium storage in a functionalized coal-based microcrystal/CNT binder-free electrode. Chem Commun (Camb). 2019;55(55):7954.
37. Cao K, Jiao L, Liu Y, Liu H, Wang Y, Yuan H. Ultra-high capacity lithium-ion batteries with hierarchical CoO nanowire clusters as binder free electrodes. Adv Func Mater. 2015;25(7):1082–9.
38. Yuan S, Huang XL, Ma DL, Wang HG, Meng FZ, Zhang XB. Engraving copper foil to give large-scale binder-free porous CuO arrays for a high-performance sodium-ion battery anode. Adv Mater. 2014;26(14):2273.
39. Shi Y, Yang D, Yu R, Liu Y, Hao S-M, Zhang S, Qu J, Yu Z. Robust binder-free anodes assembled with ultralong mischcrystal TiO_2 nanowires and reduced graphene oxide for high-rate and long cycle life lithium-ion storage. J Power Sources. 2018;383:115.
40. Li Q, Feng Y, Wang P, Che R. Superior-capacity binder-free anode electrode for lithium-ion batteries: $Co_xMn_yNi_zO$ nanosheets with metal/oxygen vacancies directly formed on Cu foil. Nanoscale. 2019;11(11):5080.
41. Teng X, Qin Y, Wang X, Li H, Shang X, Fan S, Li Q, Xu J, Cao D, Li S. A nanocrystalline Fe_2O_3 film anode prepared by pulsed laser deposition for lithium-ion batteries. Nanoscale Res Lett. 2018;13:1. https://doi.org/10.1186/s11671-018-2475.
42. Fan S, Zhang J, Teng X, Wang X, Li H, Li Q, Xu J, Cao D, Li S, Hu H. Self-supported amorphous SnO_2/TiO_2 nanocomposite films with improved electrochemical performance for lithium-ion batteries. J Electrochem Soc. 2019;166(13):A3072.
43. Cao L, Wang D, Wang R. NiO thin films grown directly on Cu foils by pulsed laser deposition as anode materials for lithium ion batteries. Mater Lett. 2014;132:357.

44. Qin Y, Li Q, Xu J, Wang X, Zhao G, Liu C, Yan X, Long Y, Yan S, Li S. CoO-Co nanocomposite anode with enhanced electrochemical performance for lithium-ion batteries. Electrochim Acta. 2017;224:90.
45. Meng R, Hou H, Liu X, Duan J, Liu S. Binder-free combination of amorphous TiO_2 nanotube arrays with highly conductive Cu bridges for lithium ion battery anode. Ionics. 2016;22(9):1527.
46. Xing GZ, Wang Y, Wong JI, Shi YM, Huang ZX, Li S, Yang YH. Hybrid CuO/SnO_2 nanocomposites: towards cost-effective and high performance binder free lithium ion batteries anode materials. Appl Phys Lett. 2014;105(14):143905.
47. Chen W, Zhang H, Ma Z, Li S, Li Z. Binder free $Cu(OH)_2$/CuO electrodes fabricated directly on copper foils by facile large-scale production method. J Alloy Compd. 2018;762:565.
48. Li Z, Li G, Xu W, Zhou M, Xu C, Shi M, Li F, Chen L, He B. Self-integrated porous leaf-like CuO nanoplate array-based anodes for high-performance lithium-ion batteries. ChemElectroChem. 2018;5(19):2774.
49. Liang P, Zhang H, Pan B, Su Y, Wang CA, Zhong M. Binder-free carbon-coated nanocotton transition metal oxides integrated anodes by laser surface ablation for lithium-ion batteries. Surf Interface Anal. 2019;51(8):874.
50. Wang S, Ju P, Zhu Z, Zhao C. Co_3O_4/RGO/Co_3O_4 pseudocomposite grown in situ on a Co foil for high-performance supercapacitors. RSC Adv. 2016;6(102):99640.
51. López MC, Lavela P, Ortiz GF, Tirado JL. Transition metal oxide thin films with improved reversibility as negative electrodes for sodium-ion batteries. Electrochem Commun. 2013;27:152.
52. Tang Y, Hong L, Wu Q, Li J, Hou G, Cao H, Wu L, Zheng G. TiO_2**b** nanowire arrays on Ti foil substrate as three-dimensional anode for lithium-ion batteries. Electrochim Acta. 2016;195:27.
53. Bi Z, Paranthaman MP, Menchhofer PA, Dehoff RR, Bridges CA, Chi M, Guo B, Sun X, Dai S. Self-organized amorphous TiO_2 nanotube arrays on porous Ti foam for rechargeable lithium and sodium ion batteries. J Power Sources. 2013;222:461.
54. Zhao G, Sun X, Zhang L, Chen X, Mao Y, Sun K. A self-supported metal-organic framework derived Co_3O_4 film prepared by an *in-situ* electrochemically assistant process as Li ion battery anodes. J Power Sources. 2018;389:8.
55. Lee DJ, Choi J, Ryou MH, Kim CH, Lee YM, Park JK. Binder-free metal fibril-supported Fe_2O_3 anodes for high-performance lithium-ion batteries. J Mater Chem A. 2014;2(9):2906.
56. Jiang Y, Hu M, Zhang D, Yuan T, Sun W, Xu B, Yan M. Transition metal oxides for high performance sodium ion battery anodes. Nano Energy. 2014;5:60.
57. Wu M, Zhang G, Chen N, Chen W, Qiao J, Sun S. A self-supported electrode as a high-performance binder- and carbon-free cathode for rechargeable hybrid zinc batteries. Energy Storage Mater. 2020;24:272.
58. Chen LY, Hou Y, Kang JL, Hirata A, Chen MW. Asymmetric metal oxide pseudocapacitors advanced by three-dimensional nanoporous metal electrodes. J Mater Chem A. 2014;2(22):8448.
59. Liu H, Wang E, Zhang Q, Ren Y, Guo X, Wang L, Li G, Yu H. Unique 3D nanoporous/macroporous structure Cu current collector for dendrite-free lithium deposition. Energy Storage Mater. 2019;17:253.
60. Prabhin VS, Jeyasubramanian K, Jeyaseeli Rashmi I, Hikku GS, Veluswamy P, Cho BJ. Investigation of electrochemical capacitance of 18k nanoporous current collector incorporated MnO2. Mater Chem and Phys. 2018;220:128.
61. Li Y, Kong LB, Liu MC, Zhang WB, Kang L. Facile synthesis of $Co_3V_2O_8$ nanoparticle arrays on Ni foam as binder-free electrode with improved lithium storage properties. Ceram Int. 2017;43(1):1166.
62. Li H, Zu J, Zhang S, Zhu J, Liu J, Xu Y. Facile synthesis of foamed-nickel supporting MnO_2 as binder-less electrodes for high electrochemical performance supercapacitors. J Nanopart Res. 2019;21(2):34.
63. Fu Y, Li X, Sun X, Wang X, Liu D, He D. Self-supporting Co_3O_4 with lemongrass-like morphology as a high-performance anode material for lithium ion batteries. J Mater Chem. 2012;22(34):17429.
64. Huang M, Li F, Zhao XL, Luo D, You XQ, Zhang YX, Li G. Hierarchical ZnO@MnO_2 core-shell Pillar arrays on Ni foam for binder-free supercapacitor electrodes. Electrochim Acta. 2015;152:172.
65. Wu H, Sun W, Wang Y, Wang F, Liu J, Yue X, Wang Z, Qiao J, Rooney DW, Sun K. Facile synthesis of hierarchical porous three-dimensional free-standing $MnCo_2O_4$ cathodes for long-life Li-O_2 batteries. ACS Appl Mater Inter. 2017;9(14):12355.
66. Veerasubramani GK, Krishnamoorthy K, Kim SJ. Improved electrochemical performances of binder-free $CoMoO_4$ nanoplate arrays@Ni foam electrode using redox additive electrolyte. J Power Sources. 2016;306:378.
67. Wang H, Chen H, Wang H, Wu L, Wu Q, Luo Z, Wang F. Hierarchical porous $FeCo_2O_4$@Ni as a carbon- and binder-free cathode for lithium-oxygen batteries. J Alloy Compd. 2019;780:107.
68. Jiang SL, Shi TL, Long H, Sun YM, Zhou W, Tang ZR. High-performance binder-free supercapacitor electrode by direct growth of cobalt-manganese composite oxide nansostructures on nickel foam. Nanoscale Res Lett. 2014;492(9):492.
69. Zhao G, Xu Z, Sun K. Hierarchical porous Co_3O_4 films as cathode catalysts of rechargeable Li-O_2 batteries. J Mater Chem. 2013;1(41):12862.
70. Leng L, Zeng X, Song H, Shu T, Wang H, Liao S. Pd nanoparticles decorating flower-like Co_3O_4 nanowire clusters to form an efficient, carbon/binder-free cathode for Li-O_2 batteries. J Mater Chem. 2015;3(30):15626.
71. Qi J, Wang P, Yan Y, Zheng X, Cao J, Feng J. MCo_2O_4 (M=Co, Mn, Ni, Zn) nanosheet arrays constructed by two-dimension metal-organic frameworks as binder-free electrodes for lithium-ion batteries. Vacuum. 2019;169:108959.
72. Liu S, Wu J, Zhou J, Fang G, Liang S. Mesoporous $NiCo_2O_4$ nanoneedles grown on three dimensional graphene networks as binder-free electrode for high-performance lithium-ion batteries and supercapacitors. Electrochim Acta. 2015;176:1.
73. Li J, Wang X, Song S, Zhao S, Wang F, Pan J, Feng J, Zhang H. Self-supported Co_3O_4wire-penetrated-cage hybrid arrays with enhanced supercapacitance properties. CrystEngComm. 2017;19(11):1459.
74. Du Y, Ma W, Li H. In situ growth of CoP_3 / carbon polyhedron/ CoO/NF nanoarrays as binder-free anode for lithium-ion batteries with enhanced specific capacity. Small. 2020;16(11):e1907468.
75. Zhang C, Yu JS. Morphology-tuned synthesis of $NiCo_2O_4$-coated 3D graphene architectures used as binder-free electrodes for lithium-ion batteries. Chemistry. 2016;22(13):4422.
76. Kundu M, Liu L. Binder-free electrodes consisting of porous NiO nanofibers directly electrospun on nickel foam for high-rate supercapacitors. Mater Lett. 2015;144:114.
77. Yang W, Cheng G, Dong C, Bai Q, Chen X, Peng Z, Zhang Z. NiO nanorod array anchored Ni foam as a binder-free anode for high-rate lithium ion batteries. J Mater Chem A. 2014;2(47):20022.
78. Han X, Cheng F, Chen C, Li F, Chen J. A Co_3O_4@MnO_2/Ni nanocomposite as a carbon- and binder-free cathode for rechargeable Li-O_2 batteries. Inorg Chem Front. 2016;3(6):866.
79. Yuan W, Qiu Z, Chen Y, Zhao B, Liu M, Tang Y. A binder-free composite anode composed of CuO nanosheets and multi-wall carbon nanotubes for high-performance lithium-ion batteries. Electrochim Acta. 2018;267:150.
80. Liu D, Yang Z, Wang P, Li F, Wang D, He D. Preparation of 3D nanoporous copper-supported cuprous oxide for

high-performance lithium ion battery anodes. Nanoscale. 2013;5(5):1917.
81. Zhang H, Zhang X, Li H, Zhang Y, Zeng Y, Tong Y, Zhang P, Lu X. Flexible rechargeable Ni//Zn battery based on self-supported $NiCo_2O_4$ nanosheets with high power density and good cycling stability. Green Energy Environ. 2018;3(1):56.
82. Shao J, Zhou H, Zhu M, Feng J, Yuan A. Carbon cloth-supported Fe_2O_3 derived from Prussian blue as self-standing anodes for high-performance lithium-ion batteries. J Nanopart Res. 2019;21(4):79.
83. Liang K, Gu T, Cao Z, Tang X, Hu W, Wei B. In situ synthesis of SWNTs@MnO_2/polypyrrole hybrid film as binder-free supercapacitor electrode. Nano Energy. 2014;9:245.
84. Luo Y, Zhang H, Wang L, Zhang M, Wang T. Fixing graphene-Mn_3O_4 nanosheets on carbon cloth by a poles repel-assisted method to prepare flexible binder-free electrodes for supercapacitors. Electrochim Acta. 2015;180:983.
85. Wang X, Zhang M, Liu E, He F, Shi C, He C, Li J, Zhao N. Three-dimensional core-shell Fe_2O_3@ carbon/carbon cloth as binder-free anode for the high-performance lithium-ion batteries. Appl Surf Sci. 2016;390:350.
86. Cao C, Wei L, Wang G, Shen J. In-situ growing $NiCo_2O_4$ nanoplatelets on carbon cloth as binder-free catalyst air-cathode for high-performance microbial fuel cells. Electrochim Acta. 2017;231:609.
87. Wang M, Huang Y, Wang K, Zhu Y, Zhang N, Zhang H, Li S, Feng Z. PVD synthesis of binder-free silicon and carbon coated 3D α-Fe_2O_3 nanorods hybrid films as high-capacity and long-life anode for flexible lithium-ion batteries. Energy. 2018;164:1021.
88. Shen L, Che Q, Li H, Zhang X. Mesoporous $NiCo_2O_4$ nanowire arrays grown on carbon textiles as binder-free flexible electrodes for energy storage. Adv Funct Mater. 2014;24(18):2630.
89. Chen Y, Guan JH, Gan H, Chen BZ, Shi XC. Electrochemical growth of α-MnO_2 on carbon fibers for high-performance binder-free electrodes of supercapacitors. J Appl Electrochem. 2017;48(1):105.
90. Liu Y, Wang B, Sun Q, Pan Q, Zhao N, Li Z, Yang Y, Sun X. Controllable synthesis of Co@CoO_x/Helical nitrogen-doped carbon nanotubes toward oxygen reduction reaction as binder-free cathodes for Al-air batteries. ACS Appl Mater Inter. 2020;12(14):16512.
91. Ji D, Zhou H, Tong Y, Wang J, Zhu M, Chen T, Yuan A. Facile fabrication of MOF-derived octahedral CuO wrapped 3D graphene network as binder-free anode for high performance lithium-ion batteries. Chemical Eng J. 2017;313:1623.
92. Liu Y, Wang W, Gu L, Wang Y, Ying Y, Mao Y, Sun L, Peng X. Flexible CuO nanosheets/reduced-graphene oxide composite paper: binder-free anode for high-performance lithium-ion batteries. ACS Appl Mater Inter. 2013;5(19):9850.
93. Zhang X, Wang C, Chen YN, Wang XG, Xie Z, Zhou Z. Binder-free $NiFe_2O_4$/C nanofibers as air cathodes for Li-O_2 batteries. J Power Sources. 2018;377:136.
94. Wang L, Yang G, Wang J, Wang S, Wang C, Peng S, Yan W, Ramakrishna S. In situ fabrication of branched TiO_2/C nanofibers as binder-free and free-standing anodes for high-performance sodium-ion batteries. Small. 2019;15(30):e1901584.
95. Xie W, Li S, Wang S, Xue S, Liu Z, Jiang X, He D. N-doped amorphous carbon coated Fe_3O_4/SnO_2 coaxial nanofibers as a binder-free self-supported electrode for lithium ion batteries. ACS Appl Mater Inter. 2014;6(22):20334.
96. Jiang Y, Chen S, Mu D, Zhao Z, Li C, Ding Z, Xie C, Wu F. Flexible TiO_2/SiO_2/C film anodes for lithium-ion batteries. Chemsuschem. 2018;11(13):2040.
97. Que LF, Yu FD, Wang ZB, Gu DM. Pseudocapacitance of TiO_{2-x}/CNT anodes for high-performance quasi-solid-state Li-ion and Na-ion capacitors. Small. 2018;14(17):e1704508.
98. Wang Y, Guo J, Li L, Ge Y, Li B, Zhang Y, Shang Y, Cao A. High-loading Fe_2O_3/SWNT composite films for lithium-ion battery applications. Nanotechnology. 2017;28(34):345703.
99. Luo SH, Hu DB, Liu H, Li JZ, Yi TF. Hydrothermal synthesis and characterization of alpha-Fe_2O_3/C using acid-pickled iron oxide red for Li-ion batteries. J Hazard Mater. 2019;368:714.
100. Zhou T, Xu W, Zhang N, Du Z, Zhong C, Yan W, Ju H, Chu W, Jiang H, Wu C, Xie Y. Ultrathin cobalt oxide layers as electrocatalysts for high-performance flexible Zn-air batteries. Adv Mater. 2019;31(15):e1807468.
101. Wang X, Liao Z, Fu Y, Neumann C, Turchanin A, Nam G, Zschech E, Cho J, Zhang J, Feng X. Confined growth of porous nitrogen-doped cobalt oxide nanoarrays as bifunctional oxygen electrocatalysts for rechargeable zinc–air batteries. Energy Storage Mater. 2020;26:157.
102. Ma L, Chen S, Pei Z, Li H, Wang Z, Liu Z, Tang Z, Zapien JA, Zhi C. Flexible waterproof rechargeable hybrid zinc batteries initiated by multifunctional oxygen vacancies-rich cobalt oxide. ACS Nano. 2018;12(8):8597.
103. Susantyoko RA, Wang X, Xiao Q, Fitzgerald E, Zhang Q. Sputtered nickel oxide on vertically-aligned multiwall carbon nanotube arrays for lithium-ion batteries. Carbon. 2014;68:619.
104. Zhang J, Ni S, Tang J, Yang X, Zhang L. The preparation of NiO/C-Ni composite as binder free anode for lithium ion batteries. Mater Lett. 2016;176:21.
105. Fan X, Ni K, Han J, Wang S, Gou L, Li DL. Cathodic electrodeposition of porous MnO_2 film as binder-free cathode for high performance rechargeable Zinc-ion battery. Funct Mater Lett. 2019;1:5.
106. Liu H, Guo Z, Wang S, Xun X, Chen D, Lian J. Reduced core-shell structured $MnCo_2O_4$@MnO_2 nanosheet arrays with oxygen vacancies grown on Ni foam for enhanced-performance supercapacitors. J Alloy Compd. 2020;846:156504.
107. Ozcan S, Tokur M, Cetinkaya T, Guler A, Uysal M, Guler MO, Akbulut H. Free standing flexible graphene oxide + α-MnO_2 composite cathodes for Li–air batteries. Solid State Ionics. 2016;286:34.
108. Aqueel Ahmed AT, Hou B, Inamdar AI, Cha S, Kim H, Im H. Morphology engineering of self-assembled nanostructured $CuCo_2O_4$ anodes for lithium-ion batteries. Energy Technol-ger. 2019;7(7):1900295.
109. Zhang H, Tang Z, Zhang K, Wang L, Shi H, Zhang G, Duan H. Pseudo-solid-solution $CuCo_2O_4$/C nanofibers as excellent anodes for lithium ion batteries. Electrochim Acta. 2017;247:692.
110. Li Y, Liu M, Hou S, Wang P, Pan X, Xie M, Chen Y, Zhao L. Direct growth of urchin-like $CuCo_2O_4$ on Ni foam for ultrahigh capacity and excellent rate ability of lithium ion batteries. Appl Surf Sci. 2018;458:517.
111. Li J, Zhang Y, Li L, Cheng L, Dai S, Wang F, Wang Y, Yu X. Formation of highly porous $CuCo_2O_4$ nanosheet assemblies for high-rate and long-term lithium storage. Sustain Energy Fuels. 2019;3(12):3370.
112. Jin Y, Wang L, Jiang Q, Du X, Ji C, He X. Mesoporous $MnCo_2O_4$ microflower constructed by sheets for lithium ion batteries. Mater Lett. 2016;177:85.
113. Wu L, Lang J, Wang S, Zhang P, Yan X. Study of Ni-dopped $MnCo_2O_4$ yolk-shell submicron-spheres with fast Li^+ intercalation pseudocapacitance as an anode for high-performance lithium ion batteries. Electrochim Acta. 2016;203:128.
114. Zhang L, Tang Q, Chen X, Fan B, Xiao K, Zhang S, Deng W, Hu A. Self-assembled synthesis of diamond-like $MnCo_2O_4$ as anode active material for lithium-ion batteries with high cycling stability. J Alloy Compd. 2017;722:387.
115. Yang H, Xie Y, Zhu M, Liu Y, Wang Z, Xu M, Lin S. Hierarchical porous $MnCo_2O_4$ yolk-shell microspheres from MOFs as

secondary nanomaterials for high power lithium ion batteries. Dalton Trans. 2019;48(25):9205.
116. Zhou L, Zhao D, Lou XW. Double-shelled $CoMn_2O_4$ hollow microcubes as high-capacity anodes for lithium-ion batteries. Adv Mater. 2012;24(6):745.
117. Bijelić M, Liu X, Sun Q, Djurišić AB, Xie MH, Ng AMC, Suchomski C, Djerdj I, Skoko Z, Popović J. Long cycle life of $CoMn_2O_4$ lithium ion battery anodes with high crystallinity. J Mater Chem A. 2015;3(28):14759.
118. Pan X, Ma J, Yuan R, Yang X. Layered double hydroxides for preparing $CoMn_2O_4$ nanoparticles as anodes of lithium ion batteries. Mater Chemi and Phys. 2017;194:137.
119. Chen R, Hu Y, Shen Z, Chen Y, He X, Zhang X, Zhang Y. Controlled synthesis of carbon nanofibers anchored with $Zn_xCo_{3-x}O_4$ nanocubes as binder-free anode materials for lithium-ion batteries. ACS Appl Mater Inter. 2016;8(4):2591.
120. Zhang G, Yu L, Wu HB, Hoster HE, Lou XW. Formation of $ZnMn_2O_4$ ball-in-ball hollow microspheres as a high-performance anode for lithium-ion batteries. Adv Mater. 2012;24(34):4609.
121. Zhang T, Qiu H, Zhang M, Fang Z, Zhao X, Wang L, Chen G, Wei Y, Yue H, Wang C, Zhang D. A unique 2D-on-3D architecture developed from $ZnMn_2O_4$ and CMK-3 with excellent performance for lithium ion batteries. Carbon. 2017;123:717.
122. Zhang T, Yue H, Qiu H, Wei Y, Wang C, Chen G, Zhang D. Nano-particle assembled porous core-shell $ZnMn_2O_4$ microspheres with superb performance for lithium batteries. Nanotechnology. 2017;28(10):105403.
123. Pang F, Hou S, Wang P, Liu M, Luo Y, Zhao L. β-MnO_2/metal-organic framework derived nanoporous $ZnMn_2O_4$ nanorods as lithium-ion battery anodes with superior lithium-storage performance. Chemistry. 2019;25(19):5043.
124. Gong F, Xia D, Bi C, Yang J, Zeng W, Chen C, Ding Y, Xu Z, Liao J, Wu M. Systematic comparison of hollow and solid $Co_3V_2O_8$ micro-pencils as advanced anode materials for lithium ion batteries. Electrochim Acta. 2018;264:358.
125. Zhang Q, Pei J, Chen G, Bie C, Chen D, Jiao Y, Rao J. $Co_3V_2O_8$ hexagonal pyramid with tunable inner structure as high performance anode materials for lithium ion battery. Electrochim Acta. 2017;238:227.
126. Sambandam B, Soundharrajan V, Mathew V, Song J, Kim S, Jo J, Tung DP, Kim S, Kim J. Metal-organic framework-combustion: a new, cost-effective and one-pot technique to produce a porous $Co_3V_2O_8$ microsphere anode for high energy lithium ion batteries. J Mater Chem A. 2016;4(38):14605.
127. Park JS, Kim JH, Kang YC. Synthesis of carbonaceous/carbon-free nanofibers consisted of $Co_3V_2O_8$ nanocrystals for lithium-ion battery anode with ultralong cycle life. Electrochim Acta. 2019;313:48.
128. Peng L, Zhang H, Bai Y, Yang J, Wang Y. Unique synthesis of mesoporous peapod-like $NiCo_2O_4$–C nanorods array as an enhanced anode for lithium ion batteries. J Mater Chem A. 2015;3(44):22094.
129. Zhang J, Chen Y, Chu R, Jiang H, Zeng Y, Zhang Y, Huang N, Guo H. Pseudocapacitive P-doped $NiCo_2O_4$ microspheres as stable anode for lithium ion batteries. J Alloy Compd. 2019;787:1051.
130. Wang J, Zhang H, Lv X, Nie K, Gao X, Zhong J, Sun X. Self-supported ultrathin mesoporous $CoFe_2O_4$/CoO nanosheet arrays assembled from nanowires with enhanced lithium storage performance. J Mater Sci. 2016;51(14):6590.
131. Ambade RB, Koh KH, Ambade SB, Eom W, Noh SH, Koo CM, Kim SH, Han TH. Kinetically controlled low-temperature solution-processed mesoporous rutile TiO_2 for high performance lithium-ion batteries. J Ind Eng Chem. 2019;80:667.
132. Choi T, Kim SD, Yeo S, Cheon T, Kim SH, Ahn JH, Kim H. Rate performance enhancement of lithium-ion battery using precise thickness-controllable-carbon-coated titanium dioxide nanowire array electrode via atomic layer deposition. Electrochim Acta. 2020;334:135596.
133. Choi WH, Lee CH, Kim He, Lee SU, Bang JH. Designing a high-performance nitrogen-doped titanium dioxide anode material for lithium-ion batteries by unravelling the nitrogen doping effect. Nano Energy. 2020;74:104829.
134. Fasakin O, Oyedotun KO, Kebede M, Rohwer M, Roux LL, Mathe M, Eleruja MA, Ajayi EOB, Manyala N. Preparation and physico-chemical investigation of anatase TiO_2 nanotubes for a stable anode of lithium-ion battery. Energy Reports. 2020. https://doi.org/10.1016/j.egyr.2020.02.010.
135. Gardecka AJ, Lübke M, Armer CF, Ning D, Reddy MV, Williams AS, Lowe A, Liu Z, Parkin IP, Darr JA. Nb-doped rutile titanium dioxide nanorods for lithium-ion batteries. Solid State Sci. 2018;83:115.
136. Guo C, Tian Q, Yang L. The size-controllable spindle TiO_2 nanograins and their lithium storage properties. J Alloy Compd. 2019;776:740.
137. Ha JU, Lee J, Abbas MA, Lee MD, Lee J, Bang JH. Designing hierarchical assembly of carbon-coated TiO_2 nanocrystals and unraveling the role of TiO_2/Carbon Interface in lithium-ion storage in TiO_2. ACS Appl Mater Inter. 2019;11(12):11391.
138. Ji W, Mei Y, Yang M, Liu H, Wang S, Shan Z, Fei D, Liu X, Gao X, Li X. The core-shell mesoporous titanium dioxide with *in-situ* nitrogen doped carbon as the anode for high performance lithium-ion battery. J Alloy Compd. 2019;1:806–946.
139. Jo MS, Park GD, Kang YC, Cho JS. Design and synthesis of interconnected hierarchically porous anatase titanium dioxide nanofibers as high-rate and long-cycle-life anodes for lithium-ion batteries. Nanoscale. 2018;10(28):13539.
140. Li H, Li L, Zheng S, Wang X, Ma Z. High temperature resistant separator of PVDF-HFP/DBP/C-TiO_2 for lithium-ion batteries. Materials (Basel). 2019;12(17):2813.
141. Zhou F, Ouyang L, Liu J, Yang XS, Zhu M. Chemical bonding black phosphorus with TiO_2 and carbon toward high-performance lithium storage. J Power Sources. 2020;449:227549.
142. Zhong W, Huang J, Liang S, Liu J, Li Y, Cai G, Jiang Y, Liu J. New prelithiated V_2O_5 superstructure for lithium-ion batteries with long cycle life and high power. ACS Energy Lett. 2019;5(1):31.
143. Li L, Li Z, Yoshimura A, Sun C, Wang T, Chen Y, Chen Z, Littlejohn A, Xiang Y, Hundekar P, Bartolucci SF, Shi J, Shi S, Meunier V, Wang G, Koratkar N. Vanadium disulfide flakes with nanolayered titanium disulfide coating as cathode materials in lithium-ion batteries. Nat Commun. 2019;10(1):1764.
144. Mao W, Wang Z, Li C, Zhu X, Dai C, Yang H, Chen X, Fang D. *In-situ* characterizations of chemo-mechanical behavior of free-standing vanadium pentoxide cathode for lithium-ion batteries during discharge-charge cycling using digital image correlation. J Power Sources. 2018;402:272.
145. Nakhanivej P, Park SK, Shin KH, Yun S, Park HS. Hierarchically structured vanadium pentoxide/reduced graphene oxide composite microballs for lithium ion battery cathodes. J Power Sources. 2019;436:226854.
146. Wang Y, Nie Z, Pan A, Zhang Y, Kong X, Zhu T, Liang S, Cao G. Self-templating synthesis of double-wall shelled vanadium oxide hollow microspheres for high-performance lithium ion batteries. J Mater Chem A. 2018;6(16):6792.
147. Yao J, Li Y, Massé RC, Uchaker E, Cao G. Revitalized interest in vanadium pentoxide as cathode material for lithium-ion batteries and beyond. Energy Storage Mater. 2018;11:205.

148. Song S, Huang Q, Zhu W. Hydrothermal route to VO_2(B) nanorods: controlled synthesis and characterization. J Nanopart Res. 2017;19(10):353.
149. Rahman MM, Wang JZ, Idris NH, Chen Z, Liu H. Enhanced lithium storage in a VO_2(B)-multiwall carbon nanotube microsheet composite prepared via an in situ hydrothermal process. Electrochim Acta. 2010;56(2):693.
150. Pei C, Xiong F, Sheng J, Yin Y, Tan S, Wang D, Han C, An Q, Mai L. VO_2 nanoflakes as the cathode material of hybrid magnesium-lithium-ion batteries with high energy density. ACS Appl Mater Inter. 2017;9(20):17060.
151. Ma Y, Huang A, Zhou H, Ji S, Zhang S, Li R, Yao H, Cao X, Jin P. Template-free formation of various V_2O_5 hierarchical structures as cathode materials for lithium-ion batteries. J Mater Chem A. 2017;5(14):6522.
152. Luo T, Liu Y, Su H, Xiao R, Huang L, Xiang Q, Zhou Y, Chen C. Nanostructured- VO_2(B): a high-capacity magnesium-ion cathode and its electrochemical reaction mechanism. Electrochim Acta. 2018;260:805.
153. Gu L, Wang J, Ding J, Li B, Yang S. W-doped VO_2(B) nanosheets-built 3D networks for fast lithium storage at high temperatures. Electrochim Acta. 2019;295:393.
154. He G, Li L, Manthiram A. VO_2/rGO nanorods as a potential anode for sodium- and lithium-ion batteries. J Mater Chem A. 2015;3(28):14750.
155. Guo W, Wang Y, Li Q, Wang D, Zhang F, Yang Y, Yang Y. SnO_2@C@VO_2 composite hollow nanospheres as an anode material for lithium-ion batteries. ACS Appl Mater Inter. 2018;10(17):14993.
156. Li S, Liu G, Liu J, Lu Y, Yang Q, Yang LY, Yang HR, Liu S, Lei M, Han M. Carbon fiber cloth@VO_2(B): excellent binder-free flexible electrodes with ultrahigh mass-loading. J Mater Chem A. 2016;4(17):6426.
157. Yuan W, Luo J, Pan B, Qiu Z, Huang S, Tang Y. Hierarchical shell/core CuO nanowire/carbon fiber composites as binder-free anodes for lithium-ion batteries. Electrochim Acta. 2017;241:261.
158. Ning H, Xie H, Zhao Q, Liu J, Tian W, Wang Y, Wu M. Electrospinning ZnO/carbon nanofiber as binder-free and self-supported anode for Li-ion batteries. J Alloy Compd. 2017;722:716.
159. Samdani JS, Kang TH, Zhang C, Yu JS. Bicontinuous spider network architecture of free-standing $MnCoO_X$@NCNF anode for Li-ion battery. ACS Omega. 2017;2(11):7672.
160. Ma X, Li Z, Chen D, Li Z, Yan L, Li S, Liang C, Ling M, Peng X. Nitrogen-doped porous carbon sponge-confined ZnO quantum dots for metal collector-free lithium ion battery. J Electroanal Chem. 2019;848:113275.
161. Wang X, Liu Y, Wang Y, Jiao L. CuO quantum dots embedded in carbon nanofibers as binder-free anode for sodium ion batteries with enhanced properties. Small. 2016;12(35):4865.
162. Liu J, Dai J, Huang L, Fu B. Flexible and binder-free electrospun Co_3O_4 nanoparticles/carbon composite nanofiber mats as negative electrodes for sodium-ion batteries. Funct Mater Lett. 2018;11(04):1850072.
163. Wang X, Cao K, Wang Y, Jiao L. Controllable N-doped $CuCo_2O_4$@C film as a self-supported anode for ultrastable sodium-ion batteries. Small. 2017;13(29):1700873.
164. Song MJ, Kim IT, Kim YB, Shin MW. Self-standing, binder-free electrospun Co_3O_4/carbon nanofiber composites for non-aqueous Li-air batteries. Electrochim Acta. 2015;182:289.
165. Gomez J, Kalu EE, Nelson R, Weatherspoon MH, Zheng JP. Binder-free Co–Mn composite oxide for Li–air battery electrode. J Mater Chem A. 2013;1(10):3287.
166. Huang M, Mi R, Liu H, Li F, Zhao XL, Zhang W, He S, Zhang Y. Layered manganese oxides-decorated and nickel foam-supported carbon nanotubes as advanced binder-free supercapacitor electrodes. J Power Sources. 2014;269:760.
167. Tian D, Lu X, Nie G, Gao M, Song N, Wang C. Growth of polyaniline thorns on hybrid electrospun CNFs with nickel nanoparticles and graphene nanosheets as binder-free electrodes for high-performance supercapacitors. Appl Surf Sci. 2018;458:389.
168. Gao Z, Zhang L, Chang J, Wang Z, Wu D, Xu F, Guo Y, Jiang K. $ZnCo_2O_4$-reduced graphene oxide composite with balanced capacitive performance in asymmetric supercapacitors. Appl Surf Sci. 2018;442:138.
169. Chen SM, Yang G, Jia Y, Zheng HJ. Three-dimensional $NiCo_2O_4$@$NiWO_4$ core–shell nanowire arrays for high performance supercapacitors. J Mater Chem A. 2017;5:1028.
170. Hwang JY, Du HL, Yun BN, Jeong MG, Kim JS, Kim H, Jung HG, Sun YK. Carbon-free TiO_2 microspheres as anode materials for sodium ion batteries. ACS Energy Lett. 2019;4(2):494.
171. Liang J, Zhang L, XiLi D, Kang J. Rational design of hollow tubular SnO_2@TiO_2 nanocomposites as anode of sodium ion batteries. Electrochim Acta. 2020;341:136030.
172. Wang W, Liu Y, Wu X, Wang J, Fu L, Zhu Y, Wu Y, Liu X. Advances of TiO_2 as negative electrode materials for sodium-ion batteries. Adv Mater Technol-us. 2018;3(9):1800004.
173. Xu ZL, Lim K, Park KY, Yoon G, Seong WM, Kang K. Engineering solid electrolyte interphase for pseudocapacitive anatase TiO_2 anodes in sodium-ion batteries. Adv Funct Mater. 2018;28(29):1802099.
174. Yan D, Pan LA new sodium storage mechanism of TiO_2 for sodium ion batteries. Inorg Chem Front. 2016;3(4):464.
175. Shen J, Hu W, Li Y, Li L, Lv XJ, Zhang L. Fabrication of free-standing N-doped carbon/TiO_2 hierarchical nanofiber films and their application in lithium and sodium storages. J Alloy Compd. 2017;701:372.
176. Liu X, Tan Y, Wang W, Li C, Seh ZW, Wang L, Sun Y. Conformal prelithiation nanoshell on $LiCoO_2$ enabling high-Energy lithium-ion batteries. Nano Lett. 2020;20(6):4558.
177. Lyu Y, Wu X, Wang K, Feng Z, Cheng T, Liu Y, Wang M, Chen R, Xu L, Zhou J, Lu Y, Guo B. An overview on the advances of LiCoO2 cathodes for lithium-ion batteries. Adv Energy Mater. 2020;1:2000982.
178. Zhang G, He Y, Feng Y, Wang H, Zhu X. Pyrolysis-ultrasonic-assisted flotation technology for recovering graphite and $LiCoO_2$ from spent lithium-ion batteries. ACS Sustain Chem Eng. 2018;6(8):10896.
179. Wu C, Gu S, Zhang Q, Bai Y, Li M, Yuan Y, Wang H, Liu X, Yuan Y, Zhu N, Wu F, Li H, Gu L, Lu J. Electrochemically activated spinel manganese oxide for rechargeable aqueous aluminum battery. Nat Commun. 2019;10(1):73.
180. Wu Y, Gong M, Lin MC, Yuan C, Angell M, Huang L, Wang DY, Zhang X, Yang J, Hwang BJ, Dai H. 3D graphitic foams derived from chloroaluminate anion intercalation for ultrafast aluminum-ion battery. Adv Mater. 2016;28(41):9218.
181. Yu X, Wang B, Gong D, Xu Z, Lu B. Graphene nanoribbons on highly porous 3D graphene for high-capacity and ultrastable Al-ion batteries. Adv Mater. 2017;29(4):1604118.
182. Yu Z, Jiao S, Li S, Chen X, Song WL, Teng T, Tu J, Chen H, Zhang G, Fang D. Flexible stable solid-state Al-ion batteries. Adv Funct Mater. 2019;29(1):1806799.
183. Xiao X, Wang M, Tu J, Luo Y, Jiao S. Metal–organic framework-derived Co_3O_4@MWCNTs polyhedron as cathode material for a high-performance aluminum-ion battery. ACS Sustain Chem Eng. 2019;7(19):16200.
184. Cai Y, Kumar S, Chua R, Verma V, Yuan D, Kou Z, Ren H, Arora H, Srinivasan M. Bronze-type vanadium dioxide holey nanobelts as high performing cathode material for aqueous aluminium-ion batteries. J Mater Chem A. 2020;8(25):12716.

185. Kazazi M, Abdollahi P, Mirzaei-Moghadam M. High surface area TiO_2 nanospheres as a high-rate anode material for aqueous aluminium-ion batteries. Solid State Ionics. 2017;300:32.
186. Zhang K, Lee TH, Cha JH, Jang HW, Choi JW, Mahmoudi M, Shokouhimehr M. Metal-organic framework-derived metal oxide nanoparticles@reduced graphene oxide composites as cathode materials for rechargeable aluminium-ion batteries. Sci Rep. 2019;9(1):13739.
187. Pal D, Mathur A, Singh A, Pakhira S, Singh R, Chattopadhyay S. Binder-free ZnO cathode synthesized via ALD by direct growth of hierarchical ZnO nanostructure on current collector for high-performance rechargeable aluminium-ion batteries. ChemistrySelect. 2018;3(44):12512.
188. Liu Q, Wang L, Liu X, Yu P, Tian C, Fu H. N-doped carbon-coated Co_3O_4 nanosheet array/carbon cloth for stable rechargeable Zn-air batteries. Sci China Mater. 2018;62(5):624.
189. Liu S, Gao S, Cui B, Xiang W, Liu X, Han W, Zhang J. An amorphous MnO_2/lithiated NiO nanosheet array as an efficient bifunctional electrocatalyst for iron molten air batteries. Energy Technol-ger. 2019;7(5):1800932.
190. Cao X, Sun Z, Zheng X, Jin C, Tian J, Li X, Yang R. $MnCo_2O_4$/MoO_2 nanosheets grown on Ni foam as carbon- and binder-Free cathode for lithium-oxygen batteries. Chemsuschem. 2018;11(3):574.
191. Yu L, Hu L, Anasori B, Liu YT, Zhu Q, Zhang P, Gogosti Y, Xu B. MXene-bonded activated carbon as a flexible electrode for high-performance supercapacitors. ACS Energy Lett. 2018;3(7):1597.
192. Gurten Inal II, Aktas Z. Enhancing the performance of activated carbon based scalable supercapacitors by heat treatment. Appl Surf Sci. 2020;514:145895.
193. Wang C, Wang J, Wu W, Qian J, Song S, Yue Z. Feasibility of activated carbon derived from anaerobic digester residues for supercapacitors. J Power Sources. 2019;412:683.
194. El-Kady MF, Shao Y, Kaner RB. Graphene for batteries, supercapacitors and beyond. Nat Rev Mater. 2016;1(7):16033.
195. Subramanian S, Johny MA, Malamal Neelanchery M, Ansari S. Self-discharge and voltage recovery in graphene supercapacitors. IEEE T Power Electr. 2018;33(12):10410.
196. Liu T, Liu G. Block copolymer-based porous carbons for supercapacitors. J Mater Chem A. 2019;7(41):23476.
197. Yoo Y, Kim MS, Kim JK, Kim YS, Kim W. Fast-response supercapacitors with graphitic ordered mesoporous carbons and carbon nanotubes for AC line filtering. J Mater Chem A. 2016;4(14):5062.
198. Liu T, Zhang F, Song Y, Li Y. Revitalizing carbon supercapacitor electrodes with hierarchical porous structures. J Mater Chem A. 2017;5(34):17705.
199. Ma W, Chen S, Yang S, Chen W, Weng W, Cheng Y, Zhu M. Flexible all-solid-state asymmetric supercapacitor based on transition metal oxide nanorods/reduced graphene oxide hybrid fibers with high energy density. Carbon. 2017;113:151.
200. Tajik S, Dubal DP, Gomez-Romero P, Yadegari A, Rashidi A, Nasernejad B, Inamuddin AAM. Nanostructured mixed transition metal oxides for high performance asymmetric supercapacitors: facile synthetic strategy. Int J Hydrogen Energ. 2017;42(17):12384.
201. Wang L, Duan G, Zhu J, Chen SM, Liu XH, Palanisamy S. Mesoporous transition metal oxides quasi-nanospheres with enhanced electrochemical properties for supercapacitor applications. J Colloid Interface Sci. 2016;483:73.
202. Yang Q, Li Z, Zhang R, Zhou L, Shao M, Wei M. Carbon modified transition metal oxides/hydroxides nanoarrays toward high-performance flexible all-solid-state supercapacitors. Nano Energy. 2017;41:408.
203. Zhang G, Xiao X, Li B, Gu P, Xue H, Pang H. Transition metal oxides with one-dimensional/one-dimensional-analogue nanostructures for advanced supercapacitors. J Mater Chem A. 2017;5(18):8155.
204. Pan Z, Qiu Y, Yang J, Ye F, Xu Y, Zhang X, Liu M, Zhang Y. Ultra-endurance flexible all-solid-state asymmetric supercapacitors based on three-dimensionally coated MnO_x nanosheets on nanoporous current collectors. Nano Energy. 2016;26:610.
205. Shinde SK, Yadav HM, Ramesh S, Bathula C, Maile N, Ghodake GS, Dhaygude H, Kim DY. High-performance symmetric supercapacitor; nanoflower-like $NiCo_2O_4$//$NiCo_2O_4$ thin films synthesized by simple and highly stable chemical method. J Mol Liq. 2020;299:112119.
206. Singh A, Ojha AK. Designing vertically aligned porous $NiCo_2O_4$@$MnMoO_4$ Core@Shell nanostructures for high-performance asymmetric supercapacitors. J Colloid Interface Sci. 2020;580:720.
207. Wang WD, Zhang PP, Gao SQ, Wang BQ, Wang XC, Li M, Liu F, Cheng JP. Core-shell nanowires of $NiCo_2O_4$@alpha-$Co(OH)_2$ on Ni foam with enhanced performances for supercapacitors. J Colloid Interface Sci. 2020;579:71.
208. Wang X, Fang Y, Shi B, Huang F, Rong F, Que R. Three-dimensional $NiCo_2O_4$@$NiCo_2O_4$ core–shell nanocones arrays for high-performance supercapacitors. Chem Eng J. 2018;344:311.
209. Dong T, Li M, Wang P, Yang P. Synthesis of hierarchical tube-like yolk-shell Co_3O_4@$NiMoO_4$ for enhanced supercapacitor performance. Int J Hydrogen Energ. 2018;43(31):14569.
210. Neeraj NS, Mordina B, Srivastava AK, Mukhopadhyay K, Prasad NE. Impact of process conditions on the electrochemical performances of $NiMoO_4$ nanorods and activated carbon based asymmetric supercapacitor. Appl Surf Sci. 2019;473:807.
211. Wan L, Liu J, Li X, Zhang Y, Chen J, Du C, Xie M. Fabrication of core-shell $NiMoO_4$@MoS_2 nanorods for high-performance asymmetric hybrid supercapacitors. Int J Hydrogen Energ. 2020;45(7):4521.
212. Gao Y, Xia Y, Wan H, Xu X, Jiang S. Enhanced cycle performance of hierarchical porous sphere $MnCo_2O_4$ for asymmetric supercapacitors. Electrochim Acta. 2019;301:294.
213. Krittayavathananon A, Pettong T, Kidkhunthod P, Sawangphruk M. Insight into the charge storage mechanism and capacity retention fading of $MnCo_2O_4$ used as supercapacitor electrodes. Electrochim Acta. 2017;258:1008.
214. Pettong T, Iamprasertkun P, Krittayavathananon A, Sukha P, Sirisinudomkit P, Seubsai A, Chareonpanich M, Kongkachuichay P, Limtrakul J, Sawangphruk M. High-performance asymmetric supercapacitors of $MnCo_2O_4$ nanofibers and N-doped reduced graphene oxide aerogel. ACS Appl Mater Inter. 2016;8(49):34045.
215. Lin J, Liang H, Jia H, Chen S, Cai Y, Qi J, Cao J, Fei W, Feng J. Hierarchical $CuCo_2O_4$@$NiMoO_4$ core–shell hybrid arrays as a battery-like electrode for supercapacitors. Inorg Chem Front. 2017;4(9):1575.
216. Chen S, Zhang Z, Zeng W, Chen J, Deng L. Construction of $NiCo_2S_4$@$NiMoO_4$ core-shell nanosheet arrays with superior electrochemical performance for asymmetric supercapacitors. ChemElectroChem. 2019;6(2):590.
217. Zhang F, Su C, Wen F, Mu C, Li X, Ming X. High-performance aqueous asymmetric supercapacitors based on microwave-synthesized self-supported $NiCo_2O_4$ nanograss and carbide-derived carbon. ChemistrySelect. 2020;5(10):2865.

218. Yan D, Wang W, Luo X, Chen C, Zeng Y, Zhu ZH. $NiCo_2O_4$ with oxygen vacancies as better performance electrode material for supercapacitor. Chem Eng J. 2018;334:864.
219. Zhang GQ, Wu HB, Hoster HE, Chan-Park MB, Lou XW. Single-crystalline $NiCo_2O_4$ nanoneedle arrays grown on conductive substrates as binder-free electrodes for high-performance supercapacitors. Energ Environ Sci. 2012;5(11):9453.
220. Guo D, Luo Y, Yu X, Li Q, Wang T. High performance $NiMoO_4$ nanowires supported on carbon cloth as advanced electrodes for symmetric supercapacitors. Nano Energy. 2014;8:174.
221. Du J, Zhou G, Zhang H, Cheng C, Ma J, Wei W, Chen L, Wang T. Ultrathin porous $NiCo_2O_4$ nanosheet arrays on flexible carbon fabric for high-performance supercapacitors. ACS Appl Mater Inter. 2013;5(15):7405.
222. Qu Z, Shi M, Wu H, Liu Y, Jiang J, Yan C. An efficient binder-free electrode with multiple carbonized channels wrapped by $NiCo_2O_4$ nanosheets for high-performance capacitive energy storage. J Power Sources. 2019;41:179.

Dr. Han Hu received his Ph.D. degree from School of Chemical Engineering at Dalian University of Technology (DUT) in 2014. After carrying out postdoctoral research at Nanyang Technological University (2014-2016), Leibniz Institute for Solid State and Materials Research Dresden (2016-2017), and The University of Queensland (2017-2018), he has joined State key Lab of Heavy Oil Processing at China University of Petroleum (East China) as a full professor in 2018. He focuses his research interests on the production and surface engineering of functional materials for energy storage and conversion

Dr. Ming-Bo Wu is a professor and executive president of College of New Energy, China University of Petroleum (East China). His research interests have been focused on the development of new methodologies for the synthesis of functional carbon materials, and their uses in catalysis, energy conversion/storage and environmental protection. He has received a number of awards, including the First Class Award for achievements in technological invention from the China Petroleum and Chemical Industry Foundation, the Runners-up Award for achievements in technological invention from the Education Ministry of China, and so on. He has published more than 160 papers in peer-reviewed journals.